

Highly structured populations of copepods at risk to deep-sea mining: Integration of genomic data with demogenetic and biophysical modelling

Coral Diaz-recio Lorenzo ^{1,*}, Tran lu y Adrien ², Brunner Otis ³, Martinez Arbizu Pedro ⁴, Jollivet Didier ¹, Laurent Stefan ⁵, Gollner Sabine ^{6,7}

¹ Adaptation et Diversité en Milieu Marin (AD2M), Station Biologique de Roscoff Sorbonne Université, CNRS Roscoff, France

² UMR MARBEC, University of Montpellier, IRD, Ifremer, CNRS Sète, France

³ Okinawa Institute for Science and Technology Kunigami-gun Okinawa, Japan

⁴ Senckenberg am Meer, German Centre for Marine Biodiversity Research Wilhelmshaven, Germany

⁵ BioNTech Mainz, Germany

⁶ NIOZ Royal Netherlands Institute for Sea Research and Utrecht University 't Horntje (Texel), The Netherlands

⁷ Utrecht University Utrecht, The Netherlands * Corresponding author : Lorenzo Coral Diaz-recio, email address : cdrrlc@gmail.com

Abstract :

Copepoda is the most abundant taxon in deep-sea hydrothermal vents, where hard substrate is available. Despite the increasing interest in seafloor massive sulphides exploitation, there have been no population genomic studies conducted on vent meiofauna, which are known to contribute over 50% to metazoan biodiversity at vents. To bridge this knowledge gap, restriction-site-associated DNA sequencing, specifically 2b-RADseq, was used to retrieve thousands of genome-wide single-nucleotide polymorphisms (SNPs) from abundant populations of the vent-obligate copepod *Stygiopontius lauensis* from the Lau Basin. SNPs were used to investigate population structure, demographic histories and genotype–environment associations at a basin scale. Genetic analyses also helped to evaluate the suitability of tailored larval dispersal models and the parameterization of life-history traits that better fit the population patterns observed in the genomic dataset for the target organism. Highly structured populations were observed on both spatial and temporal scales, with divergence of populations between the north, mid, and south of the basin estimated to have occurred after the creation of the major transform fault dividing the Australian and the Niufo'ou tectonic plate (350 kya), with relatively recent secondary contact events (<20 kya). Larval dispersal models were able to predict the high levels of structure and the highly asymmetric northward low-level gene flow observed in the genomic data. These results differ from most studies conducted on megafauna in the region, elucidating the need to incorporate smaller size when considering site prospecting for deep-sea exploitation of seafloor massive sulphides, and the creation of area-based management tools to protect areas at risk of local extinction, should mining occur.

Keywords : connectivity, copepods, deep-sea mining, demography, hydrothermal vents, larval dispersal modelling

1. Introduction

Genetic connectivity is essential in maintaining diversity and promoting the evolution of marine organisms, and depends on factors such as dispersal ability, reproductive traits, seafloor topology, and environmental conditions (De Wit et al., 2023; Blanchard and Gollner, 2022; Virtanen et al., 2020; Brunner et al., 2023; Pereira et al., 2023; Portanier et al., 2023; Yahagi et al., 2017; Ingels et al., 2023; Mouchi et al., 2023; Plouviez et al., 2013; 2019; Faria et al., 2021; Antich et al., 2022). High dispersal ability promotes gene flow over long distances, while seafloor topology can create physical barriers that impede movement and lead to allopatric speciation (Yahagi et al., 2017; Plouviez et al., 2013; 2019; Ingels et al., 2023). Additionally, environmental factors such as temperature, salinity, and oxygen concentrations influence species distribution, potentially resulting in

local adaptation, and ultimately sympatric speciation (Virtanen et al., 2020; Faria et al., 2021; Antich et al., 2022).

Deep-sea hydrothermal vents, found along Mid Ocean Ridges (MORs) and Back-Arc Basins (BABs), support diverse meta-communities of mega-, macro-, and meiofauna (Mullineaux et al., 2018) that exhibit deeply entwined interactions across organismal groups. The community composition, succession, functional importance, and connectivity of hydrothermal vent mega- and macrofauna has been explored since hydrothermal vents were discovered in 1977. Recently, hydrothermal vent meiofauna has gained interest due to their potentially important role in the food web (limen et al., 2007;2008; Nomaki et al., 2023), broad horizontal range of vent-endemic genera (Gollner et al., 2011;2016) and the ability of non-vent-endemic genera to adapt to an unprecedented range of hydrothermal vent conditions (Nomaki et al., 2019; Nakasugi et al., 2021). Understanding the genetic connectivity of smaller size classes in these habitats is crucial due to their ephemeral nature and potential to create isolated populations at risk of local extinctions despite observed gene flow among populations along fast and slow spreading MORs (Craddock et al., 1995; Jollivet et al., 1995; Won et al., 2003; Hurtado et al., 2004; Mullineaux et al., 2010; Bweedessee et al., 2013; Gollner et al., 2011; 2016; Breusing 2015, 2016; Teixeira et al., 2011, 2012; Breusing et al., 2016; Yahagi et al., 2019; Yearsley et al., 2020; Perez et al., 2021). The life history strategies of organisms in these environments are adapted to volcanic eruptions, exhibiting R-strategist survival mechanisms characterized by rapid growth, early maturation, high fecundity, and dispersal capabilities (Van Dover et al., 2014). Recent studies have explored the demographic history of vent megafauna populations in BABs, revealing contrasting dispersal strategies (Thaler et al., 2014;

Plouviez et al., 2019; Breusing et al., 2021; Tran Lu Y et al., 2021; Poitrimol et al., 2022). However, there is currently no research on the genomic connectivity of the meiofauna (animals between 32 μ m and 1mm in size), in particular the Dirivultidae family of copepods, which thrives on hard substrates and hydrothermal vents (Figure 1, inset).

The Dirivultidae (Siphonostomatoida) exist in the tens to hundreds of thousands of individuals per vent wherever basalt rock, hard-shelled megafauna assemblages, or patches of dead organisms creating landscapes of exoskeletons exist (Gollner et al. 2010;2016; Diaz-Recio Lorenzo et al., 2021). The Dirivultidae (Siphonostomatoida) contains at least 80 described species that have adapted to vent environments, dominating areas of high temperatures with high concentrations of hydrogen sulphide and low oxygen levels where they feed predominantly on chemoautotrophic bacteria (Gollner et al., 2016, Nomaki et al., 2019; 2023; Watanabe et al., 2021; Diaz-Recio Lorenzo et al., 2021; Nakasugi et al., 2021). They have a lecithotrophic developmental mode and likely disperse via hydrothermal plumes, settling as vent-obligate adults. Species of this family exhibit large population sizes, high levels of mitochondrial gene diversity, and demographic analysis of the latter has shown that the vast majority of Dirivultidae species are undergoing population expansion (Gollner et al., 2016; Watanabe et al., 2021, Diaz-Recio Lorenzo et al., 2023).

During the last decade, Next-Generation Sequencing technology significantly increased the possibility of obtaining large genomic datasets. However, genome-scale population genetic studies have focused mostly on flagship systems and organisms. Restriction-site associated DNA sequencing (RAD-seq) has been widely applied as an alternative to obtain

meaningful genome-wide information in the form of Single Nucleotide Polymorphisms (SNPs) and in particular, 2b-RAD (Wang et al., 2012) has the ability to target a large number of markers throughout the genome of non-model organisms. This information has now widely been applied to non-model organisms to address question about contemporary population structure as well as how populations separated and reconnected through time, by modeling the effect of migration and population growth on genetic divergence (Gutenkunst et al., 2009; Excoffier et al., 2013; Rougeux et al., 2017; De Jode et al., 2022).

The mining of polymetallic seafloor massive sulphides (SMS) poses the most significant threat to hydrothermal vent communities, resulting in short- and long-term damage, including changes in vent fluid strength and chemistry, toxic plumes, habitat removal, fragmentation, and biodiversity loss (Blasiak et al., 2020; Drazen et al., 2020; Gollner et al., 2017, 2021; Levin et al., 2020; Miller et al., 2018; Van Dover et al., 2018; Blanchard and Gollner, 2022). The impacts of this damage may extend beyond the vent realm (Blanchard and Gollner et al., 2022). Back-arc basins in the western Pacific contain high-grade SMS deposits, with historical exploration tenement blocks issued by some island states (Petersen et al., 2016; Du Preez and Fisher, 2018). However, certain Pacific Island states have imposed a 10-year moratorium on mining activities to understand the environmental and societal impacts better (Kakee, 2020). Advancing our understanding of population connectivity across species size fractions, incorporating life-history traits, evolutionary adaptations, larval dispersal modeling, and demographic modeling, can contribute to defining the vent transition zone and determining the size and location of Area-Based Management Tools (ABMTs) (Blachard and Gollner, 2022).

The resilience of hydrothermal vent meta-communities depends on the dispersal and colonization abilities of organisms, which play a crucial role in their ability to adapt and survive (Mullineaux et al., 2018). Previous studies have focused on modeling the dispersal ability of a subset of vent fauna to identify isolated populations at risk of local extinction from human disturbances (Mitarai et al., 2016; Breusing et al., 2021). However, these models have primarily considered megafaunal dispersal behavior, which differs inherently from the meiofauna due to variations in energy costs associated with their size differences (Gollner et al., 2015). This study aims to investigate the demographic connectivity of the copepod *Stygiopontius lauensis*, the most abundant deep-sea hydrothermal vent animal in the Lau basin. By utilizing genomic markers across four vent sites, we examine contemporary population structure, the relationship between genomic variation and environmental factors, and the demographic history between populations. Additionally, we assess the effectiveness of tailored larval dispersal models in predicting connectivity between nearby and distant vents within the Lau basin. This multifaceted approach allows for the identification of source and sink populations, and those most at risk to the impacts of deep-sea mining.

2. Materials and Methods

2.1 Sampling

Organisms were collected in 2016, and 2019 during the FK160407 aboard the R/V Falkor (Charles and Peter, 2016: <https://doi.org/10.7284/906664>) and the Chubacarc expedition aboard the R/V L'Atalante (Hourdez and Jollivet, 2019: <https://doi.org/10.17600/18001111>) to the Southwest Pacific back-arc basin system.

During expedition FK160407 samples were collected using the remotely operated vehicle (ROV) ROPOS, using scoops and slurp guns from *Alviniconcha* and *Ifremeria* megafaunal assemblages at the vent fields Tui Malila, ABE, and Tahi Moana. During the Chubacarc expedition aboard L'Atalante, samples were obtained using the ROV Victor 6000 using slurp guns from *Alvinichoncha* megafaunal assemblages at the Tu'i Malila, ABE, and Mangatolo vent sites (Figure 1, Table 1). Megafaunal collections were processed on board of the ship as followed: Copepods were washed off from the megafauna and retained on a 32µm sieve. Copepods collected in 2016 were fixed in 96 % Ethanol, samples collected in 2019 were fixed in 99.9 % EtOH. Copepods were identified first to family level (Dirivultidae), and then identified morphologically to species using taxonomic keys described by Gollner et al. (2010). The most abundant species, namely *Stygiopontius lauensis* was chosen for this study.

2.2 Library preparation and sequencing

All samples were given three consecutive ethanol baths to remove potential external contaminants before DNA extraction. Extractions from whole specimens were carried out using the E.Z.N.A.® Mollusc DNA Kit (omega BIO-TEK). 2µl of DNA extract were used to amplify the cytochrome C oxidase, subunit I (COI) gene, using the universal Folmer primers (Folmer et al., 1994) LCO1490 (5'GGTCAACAAATCATAAAGATATTGG'3), CO2198 (5'TAAACTTCAGGGTGACCAAAAAATCA'3), M13 tails M13F-pUC (-40) (5'GTTTTTCCCAGTCACGAC'3), M13R-pUC (-40) (5'CAGGAAACAGCTATGAC'3). PCR cycle conditions were initial denaturation for 3 minutes at 94°C followed by 40 cycles of denaturation at 30 seconds for 94°C, annealing for 45 seconds at 45°C and extension for 45 seconds for 72°C and a final extension for 2 minutes at 72°C. Samples were sequenced

with Macrogen Europe. *Cox1* was chosen as a species delimiter due to its conserved nature between species, and specimens that did not match at least 98% with *S. lauensis* when blasting COI sequences against the NCBI database were not included in the library. Out of 168 specimens barcoded, 149 matched at least 98% with *S. lauensis* and were used to construct the 2b-RAD libraries.

The library was constructed using a custom index array, and the enzyme *bgcl*. DNA extraction and library preparation was conducted at the Senckenberg Institute/German Center for Marine Biodiversity Research (DZMB). 2b-RAD was chosen due to the ability of type IIb enzymes to find a large number of restriction sites across the genome that are not error prone and the type IIb restriction enzyme *bgcl* was used due its simplistic laboratory usage. DNA was digested, shearing DNA upstream and downstream of a recognition site, resulting in fragments of a uniform size of 32 bp (Wang et al., 2012). Population-specific and individual-specific barcodes were ligated to the fragments in order to multiplex a large number of individuals, reducing the number of runs and subsequent costs. Adapter-ligated fragments were then amplified using the Fusion2X master mix, with 2X 20 cycles until 2 clear bands were visible, one containing non-ligated adapter, and a second, longer (by 32 bp) fragment containing the RAD sequence with a total fragment length of 182 bp. The longer fragments were cut from the gel and purified using the Monarch® Genomic DNA Purification Kit (New England Biolabs). Paired-end 150-bp sequencing (400 million clusters) was conducted on an Illumina Nextseq500 platform at the University Medical Centre of Utrecht University (UMC) on samples from 2016. After processing samples from 2019, paired-end 150-bp sequencing (1 billion

clusters) was conducted on an Illumina Nextseq2000 platform at UMC. Samples were demultiplexed by UMC.

2.3 De novo 2b-RAD-tag assembly, filtering, and SNP-calling

The *STACKS2.6* software module *process_radtags* (Rochette et al., 2019) was used to further demultiplex samples by the adapters used to delimit the populations, remove inline barcodes, and remove PCR duplicates. All reads had a sequence length of 32bp, a characteristic of 2b-RAD sequencing using the enzyme *bcgl*, that removes bias introduced from having to truncate reads to a uniform length. A total of 149 samples were successfully sequenced, with a mean coverage of 25 X. Samples with read depth of <5 and >80 were removed. Initial exploration of the data was conducted to observe outliers, and overall structure. This was done by comparing classic multivariate analyses that visualize data under reduced dimensions such as Principal Component Analysis (PCA), non-metric Multidimensional Scaling (nMDS) and Uniform Manifold Approximation and projection (UMAP), combined with spectral clustering, to visualize population structure.

S. laevis lives in vent environments containing a high abundance of chemoautotrophic bacteria that they also feed on (Limen et al. 2007;2008; Nomaki et al. 2019). Due to the small size of copepods, the entire specimen was used during the extraction to ensure sufficient quantities of pure DNA for digestion and adapter ligation during library preparation. It is therefore likely that some of the RAD tags retrieved may not belong to the copepod genome. RADs created with 2b-RAD are too small to be blasted against existing databases as a quality control method to eradicate non-copepod DNA. Although still under debate, significant correlations have been found between GC content and

growth temperature in thermophilic prokaryotes (Hu et al. 2022). GC pairs have an additional hydrogen bond than AT pairs, and GC-rich genomes are expected to provide additional stability to the DNA double-helix under high temperatures. For this reason, RADs belonging to those samples were filtered for GC content higher than 50 % as an extra quality control step.

We used the SNP calling software *DiscoSnpRAD* (Gauthier et al. 2020) for SNP discovery and genotyping for RAD-seq data, which uses a k-mer based approach, implementing the construction of de Bruijn graphs to find bubbles of SNPs without the loss of too much data and without the need for a reference genome. In *DiscoSnpRAD*, the variable parameter is the length of the k-mer. This was tested with lengths between 5 and 31. An optimal k of 15 was chosen, as this resulted in a Variant Calling File (VCF) with the highest number of called SNPs. SNPs were then clustered by loci using the provided post-processing scripts from *DiscoSnpRAD*. Missing data is a common characteristic of RADseq data however studies have highlighted that removing this data could lead to loss of valuable information (Chattopadhyay et al., 2014; Eaton et al. 2016; Tripp et al. 2017; Crotti et al. 2018). Such studies have also reported that setting too conservative parameters leads to detrimental loss of information and that *de novo* SNP calling should be less stringent. Missing data cutoffs were therefore set to 0.5. This method was compared to the classic SNP calling STACKS2 software and results are available in supplementary information (S1, figures 1 and 2).

2.4 Outlier detection for structure analyses

Loci under selection are expected to behave differently from neutral loci in terms of population-related patterns of diversification and are thus typically removed from the global dataset in population genomics studies for investigation of geographic structure (Beaumont and Nichols, 1996; Luikart et al. 2003; Holderegger and Wagner, 2006; Foll and Gaggiotti, 2008; Whitlock and Lotterhos, 2015; Benestan et al. 2016; François et al. 2016; Gagnaire and Gaggiotti, 2016; Dalongeville et al. 2018). However, some studies have used outliers to investigate subtle geographic breaks in populations when local adaptation is not overcome by migration (Milano et al., 2013; Araneda et al., 2016; Dorant et al., 2022; Tran Lu Y et al., 2021). Outliers were identified using four different methods. Firstly, the population based *Bayescan v.2.1* (Foll and Gaggiotti, 2008) was used to identify markers deviating significantly from distributions of F_{st} values across all loci (alpha = 0.05) corrected for false positives using q -values (qvalue v.2.3.0, Storey et al. 2003). Secondly, *Arlequin v.3.5.2.2* (Excoffier & Lischer, 2010), was used to identify outlier SNPs based on F_{st} values calculated over all the loci, the p -values of which were significantly different from the mean (alpha = 0.05). Thirdly, the individual based *PCAdapt v.4.3.3* (Luu et al. 2017) was used to look for loci that are atypically (i.e., not geographically) related to population structure as measured by latent factors also corrected for with q -value cutoffs. A Venn diagram was created to visualize the intersection of outliers detected by all methods software.

2.5 Population structure and diversity

The *SNPRelate* package Zheng et al. (2012) in R v.4.2.3. was used to calculate the minor allele frequencies which were converted into distance matrices for use with dimension-reducing analysis as well as for calculating Identity by State (IBS). Non-metric Multidimensional Scaling (nMDS) was used to visualize the genomic structure of populations. This was compared to other methods to check whether structure was preserved across different dimension reducing techniques such as PCA and Uniform Manifold Approximation and Projection (UMAP), a non-linear dimension-reducing technique that preserves a global structure whilst revealing hidden or complex non-linear features in genomic data (Diaz-Papkovich et al. 2019; 2020). The latter was paired with Monte Carlo Reference-based Consensus Clustering (*MCRCC*) v.1.2.0 (John et al., 2020) to obtain statistics for the optimal number of genetic clusters (S2, figure 2). *ADMIXTURE* v.1.3.0 (Alexander and Lange, 2011) was used to assign ancestry to each individual based on cross validation error, where the lowest cross validation value denotes the optimal number of clusters. Analysis of Molecular Variance (*AMOVA*, Excoffier et al. 1992) was conducted in *Arlequin* v.3.5.2.2 (Excoffier & Lischer, 2010) to check for significant differences between and within populations (10,000 permutations, missing data cutoff = 20%), as well as to obtain statistics for pairwise fixation indices (F_{st}). Nucleotide diversity (π) was calculated with the population module of *STACKS2* using all sites from all 2b-RAD-tags (S1, table 1). Observed heterozygosity was calculated using the *vcfR* package (Knaus et al., 2017) in R.

2.7 Demogenetic connectivity

Population history reconstruction was conducted to investigate demogenetic connectivity. This was done using a modified version of *∂a∂i* that uses a dual annealing optimization function in the diffuse approximation to simulate and optimize the joint allele frequency of pairs of populations under different demogenetic scenarios (scripts can be found at (https://github.com/Atranluy/Scripts-Ifremeria/tree/Main/Dadi_scripts)). Modeling was performed using the observed folded joint allele frequency spectrum (JAFS) on pairs of populations that had an F_{st} value equal to or greater than 0.1. Twenty eight demographic models, described in Rougoux et al. (2017), were simulated ranging from a low to a high complexity of population parameters (S9, figure 9). The models include strict isolation (SI), isolation with migration (IM), ancient migration (AM), and secondary contact (SC), derived from an ancestral population of N_{anc} size that split into two daughter populations of sizes N_1 and N_2 with or without demographic changes. The size of the ancestral populations is calculated as follows:

$$N_{anc} = \frac{\theta_{anc}}{4 * \mu * L}$$

Where μ , represents the mutation rate per site and generation and L represents the total length of the DNA sequence used in *∂a∂i*:

$$L = \frac{z * y * 32}{x},$$

where x represents the initial total number of SNPs that were detected on y loci of 32 bp; and z represents the number of SNPs used in the $\partial a \partial i$ analyses (see Tran Lu Y et al., 2022). Time (in years) of divergence (T_{div}) in the SC model was then calculated as:

$$T_{div} = \frac{2N_{anc} (T_s + T_{sc})}{33},$$

where T_s represents the time (in generations: Time in coalescent units multiplied by $2N_{anc}$) from the secondary contact to the initial split between the populations, T_{sc} represents the time (in generations: : Time in coalescent units multiplied by $2N_{anc}$) from present to the secondary contact, and 33 in the number of generations per year. A mutation rate of 10^{-9} was used, based on updated reports of genomic substitution rates vs mutation rates for the crustacea including the Copepoda (Thomas et al., 2020). Statistics pertaining to each parameter were computed with each run, and those computed for the best model are reported. The uncertainty of the parameters of the best model computed by $\partial a \partial i$ was realized using the Fisher information matrix (FIM), considering our markers independent. FIM uncertainty was achieved with an epsilon = 0.001 from which all standard deviations and subsequent confidence intervals were calculated. Effective Population Size (N_e) was calculated using the formula:

$$N_e = Nu * b * N_{anc},$$

where Nu refers to the daughter population size and b represents the growth factor during population size change. Migration rates (M_{ij} : number of migrants exchanged per generation as calculated by $\partial a \partial i$ in coalescent units), were calculated as follows:

$$M_{ij} = (Nu * b * m1 < -2)/2,$$

Where $m1 < -2$, is the migration rate from population 2 to population 1.

2.8 Suitability of larval dispersal models in predicting empirical patterns of gene flow in genomic datasets

To investigate the direction and relative strength of migration between different localities, we generated migration networks using the *divMigrate* function (Sundqvist et al., 2016) from the R package *diveRsity* (Keenan et al., 2013) under the null hypothesis of an n-islands model without demographic changes. We used the relative number of migrants (Nm) to infer directional gene flow as an index between 0 and 1, where 0 indicates almost no migrants/generation, and 1 indicates one migrant/generation being transported from population A to population B (Sundqvist et al., 2016). Significant asymmetry was calculated by resampling with 1,000 bootstraps. Migration was calculated as a relative value, by comparing either G_{st} of Joost's D estimates between pairs of populations and a hypothetical pool of migrants, allowing for the identification of source and sink populations.

Larval dispersal simulations, using Lagrangian particle tracking methods, were conducted using Python version 3.10.2 (<http://www.python.org>) and PARCELS version 2.3.1 (Delandmeter and Sebillie, 2019). Lagrangian particle tracking, in this case, refers to the advection and diffusion of simulated particles based on the velocity of currents within an Ocean General Circulation Model (OGCM). The OGCM in question was 'MOI GLORYS12_FREE' from MERCATOR, which has a 1/12th of a degree horizontal resolution and daily temporal resolution at 50 depth bands from 0.5 to 5728m depth. Particles were advected by the Northward and Eastward vertical velocities within the OGCM and effected by horizontal diffusion (Smagorinsky, 1963) to approximate sub grid scale currents. Particles were attributed a larval behaviour so that they would approximate the planktonic nauplii of *S. lauensis*. The principal behaviour attributed to these particles was a temperature dependent Larval Dispersal Duration (LDD). Each particle interacted with OGCM temperature data via an equation to calculate LDD, adapted from O'Connor *et al.* (2007) following the methods of Mitarai *et al.* (2016) and Breusing *et al.* (2021). For *S. lauensis*, we assumed a generational turnover of 33 per year (LDD of 11 days) at 20°C and 10 per year (LDD of 36.5 days) at 10°C (Huntley *et al.*, 1991; Gollner *et al.*, 2016) to calculate the magnitude of the relationship between LDD and temperature using the equations of O'Connor *et al.* (2007). Particles were released at the location of the vent fields 100m above the seabed to replicate the entrainment of larvae into vent plumes (Ivanenko and Martinez Arbizu, 2007; Gollner *et al.*, 2015). One hundred particles were simultaneously released from these locations every four hours for six years (2010 – 2016), resulting in a total of 876,000 particles released from each vent field. We used the horizontal distribution of particles at the time they reached their LDD as a measure of larval dispersal potential. We then extrapolated this distribution using a Lagrangian

Probability Density Function (PDF) to calculate the horizontal distribution of dispersal probability. The probability densities can be interpreted as the likelihood that a particle settles in a given location where the density values are proportional (Siegel et al., 2023), smoothed across latitude and longitude using a Gaussian distribution. By extracting the value of the PDF from each vent field at the location of all other vents, we determined the probability of dispersal among all pairs of vent fields in both directions following the methods of Mitarai *et al.* (2009; 2016). Where possible, we implemented the simulation parameters recommended by the authors of PARCELS (Delandmeter and Sebillie, 2019), and provide the detailed simulation parameters in supplementary information (S10, table 4).

2.9 Genotype-Environment Association Analysis (GEAA)

The relationship between genotypes and environmental factors was investigated using *Samβada*, a genome-environment association (GEA) software designed to search for signatures of local adaptation (Duruz et al. 2019). In addition, a distance-based redundancy analysis (db-RDA), combining regression and ordination was used to investigate the relationship between environmental variables and genotypes as per Benestan, Ferchaud, et al. (2016) and Benestan, Quinn, et al. (2016). A spatial eigenfunction analysis was used to evaluate the relative contribution of geographic distance and asymmetric processes driven by deep-water ocean current circulation to genotype frequency variation in the genomic dataset. Firstly, a distance-based Moran's eigenvector map (db-MEMs) (Legendre et al. 2013), was created to decompose the Euclidean (geographic) distances between sites into vectors (db-MEMs) that can be used for subsequent analysis based on a distance matrix. The matrix consists of Euclidean

distances calculated at a depth of 1800m, the average depth at which hydrothermal plumes were found to travel in the Lau basin (Speer and Thurnherr, 2012), and therefore the depth at which *S. lauensis* may disperse (Gollner et al. 2015). These additional variables account for spatial autocorrelation and allow for the identification of non-random structure. Further, Asymmetric Eigenvector Maps (AEMs) were generated by translating the presence of a population connection in a larval dispersal probability matrix (i.e., dispersal probability from the biophysical model > 0) between all pairs of sites into a sites-by-edge matrix. We attributed a weight to each edge, which was based on the probability of dispersal between each pair of sites derived from the biophysical model. When connectivity between a given pair of sites was greater than zero in both directions, we selected the direction with the highest probability of dispersal (Xuereb et al., 2018). The db-MEMs therefore describe the geological and bathymetric setting, while the AEMs describe dispersal based on oceanographic currents. For both db-MEMs and AEMs the larger eigenvectors model broad-scale spatial structures such as topographic features (transform faults, between the north and south or differences in the density of vents), whereas the smaller eigenvectors model fine-scale spatial structures that could describe other environmental parameters less related to geography (Dray et al., 2012). We used the package *adespatial* v.0.0-8 (Dray et al., 2017) to generate db-MEMs both types of spatial variables.

Samβada was then used to identify markers with a significant correlation to the environmental variables (figure 3, S8, figure 8), based on several statistics: firstly, a G-score compares the likelihood of modes with and without environmental parameters. Secondly, the Wald-score checks whether the effect of the environmental parameters (β_2)

is different from zero, i.e., whether an environmental parameter is associated with a significant change in genotype frequencies. Q-values were once again used to correct for false positives. Markers retained after correction were added to the Venn diagram to check if any markers were shared between outlier detection methods and genotype-environment association methods. Lastly, a db-RDA was conducted on a dataset of significant SNPs (vcf was filtered to only contain significant SNPs found by Samβada). During the model selection in a db-RDA, an adjusted R^2 statistic is used to correct for the number of explanatory variables. Akaike's Information Criterion (AIC) is then used to select the best variables, and a permutation test of F (p -value) using Analysis of Variance (AMOVA) is conducted. This allows for the testing of significance of the global model, individual parameters as well as the individual RDA axis (S8, table 3).

3. Results

3.1 *De novo assembly, filtering, and SNP-calling*

A pre-GC-filtered, *de novo* assembled dataset created using discoSnpRAD++ contained 149 individuals represented by 187,737 variant bubbles, and 104,009 SNPs. After filtering for GC, a *de novo* assembled dataset contained 84,674 variant bubbles, and 18,672 SNPs which were subsequently clustered into 9039 loci, using a k-mer length of 15 and a maximum allowed indel size of zero. The dataset contained 28.4% missing data per SNP, and 11 individuals were removed with missing data above 0.5. After filtering for heterozygosity (cut off = 0.6) and 1 SNP per locus, a final SNP dataset of bi-allelic SNPs contained 138 individuals and 5778 high quality SNPs (S4, table 2), with an average

heterozygosity of 0.2. Because high F_{st} SNPs may also be caused by drift alone (under strong demographic changes), the fact that the target organism is non-model (no existing genomic information), and the very low number of SNPs found across different outlier methods (pointing to little evidence of selection), all SNPs were retained for the structure and demogenetic analysis.

3.2 Outlier Analysis

Bayescan analysis did not identify any outliers, instead, only putatively balancing, and neutral SNPs. In contrast, Arlequin and PCAdapt identified 123 and 81 outliers, respectively, with 5 shared outliers. Samβada, which was used to explore the relationship between genotype frequencies and environmental variables (db_MEMs and AEMs), identified 671 SNPs that had a significant ($\alpha = 0.01$) correlation with environmental variables. Fifty-two of them were common between Samβada and PCAdapt, and 12 between Samβada and Arlequin. Due to the low number of SNPs identified as outliers across two or more methods, no outliers were removed from the structure or demogenetic analyses (figure 3).

3.3 Population structure and diversity

Non-metric Multidimensional Scaling identified four populations, three of which were based on geographical location, and one was based on a temporal sub-structure within the ABE hydrothermal field between sampling years 2016 and 2019 (figure 2A, S3, figure 4A, B, and C). Results were compared to PCA and UMAP with MRCC (S3, figure 4). All methods captured the same structure, statistically supported by UMAP with MRCC that

was used to account for sample size and variance. The RCSI, entropy, and consensus index, of the latter, suggest that the most significantly stable amount of genetically differentiated groups within the basin is four (S2, figure 2C, E, and F). However, UMAP does not represent genetic distances, and an nMDS approach was therefore chosen to best represent the genetic distances concordantly throughout the paper.

ADMIXTURE found the most stable number of groups to be three but with almost negligible difference between cross validation error values of 0.321, 0.319, and 0.322 for values of $k=2$, $k=3$, and $k=4$ respectively (figure 2B and S5, figure 5B, C, and D). For $k=3$, populations are highly structured across the basin from Mangatolo to Tu'i Malila with some (albeit low) level of shared ancestry. We identified three distinct genetic clusters. Cluster 1 corresponds to Tui' Malila, cluster 2 to ABE and Tahi Moana (from which we conclude shared ancestry for the two populations, (which were therefore grouped for downstream analysis) and cluster 3 to Mangatolo. These results were corroborated by *STRUCTURE* analysis, where the additional testing for $K=4$ $K=5$ did not increase the number of ancestral groups. Half of the individuals from Mangatolo, collected in 2019 have a low percentage of ancestry belonging to cluster 1, mostly represented by individuals from Tu'i Malila as is the case for the ABE samples from 2019. indicating that copepods sampled from Tu'i Malila in 2016 may have been a source to other populations sampled in 2019. These ancestral pools were therefore termed south (Tu'i Malila), mid (ABE and Tahi Moana), and north (Mangatolo).

Percentage variation was 17.7% among the populations and 82.3% within the populations, with a global AMOVA F_{st} of 0.18 ($p = <0.001$). Pairwise F_{st} values were highest

between Mangatolo and ABE(2016) ($F_{st} = 0.26, p = <0.001$), followed by Tu'i Malila and ABE(2016) ($F_{st} = 0.25, p = <0.001$), Tahi Moana and Mangatolo ($F_{st} = 0.24, p = <0.001$) and Tahi Moana and Tu'i Malila ($F_{st} = 0.24, p = < 0.001$). F_{st} values between Tahi Moana and ABE (2016) were almost zero ($F_{st} = -0.00084, p = 0.12$). The F_{st} value between Mangatolo and Tu'i Malila was 0.12 ($p = <0.001$). Interestingly, F_{st} values between Mangatolo and ABE(2019) decreased ($F_{st} = 0.05, p = <0.001$), as well as between Tu'i Malila and ABE(2019) ($F_{st} = 0.08, p = <0.001$) and increased between Tahi Moana and ABE(2019) ($F_{st} = 0.11, p = <0.001$), see table 2 for significance codes. Observed heterozygosity was 0.18, 0.12, 0.08, 0.12, and 0.24 for Tu'i Malila, ABE(2016), ABE(2019), Tahi Moana, and Mangatolo, respectively.

3.4 *Demogenetic Connectivity*

The folded joint allele frequency spectra (JAFS) display the proportion of alleles shared between the north and mid and the north and south populations for the observed data (figure 4A and 5A, respectively) and the simulated spectra for the best model (figure 4B and 5B, respectively). Secondary Contact (SC) appears to be the most appropriate model in each instance and increasing the complexity with the addition of parameters 2N (linked selection), 2m (heterogeneous migration rate across the genome) and G (population size change) improved the AIC values (figure 4E and 5E, respectively). The time of divergence between the north and mid using the best model (SC2N2mG) was calculated to be ~119 kya (UCI = 189 kya, LCI = 49 kya), with a more recent secondary contact event estimated at ~4 kya (UCI = 4.5 kya, LCI = 3.5 kya) while the time of divergence between the north and south populations using the best model (SC2N2mG) was estimated to be ~326 kya (UCI = 795 kya, LCI = 239 kya), with a recent secondary contact event estimated at ~10

kya (UCI = 17 kya, LCI = 3.2 kya). However, absolute estimates are approximately the same order of magnitude with an increase of 2.5 between them, potentially due to uncertainty in the $\partial a \partial i$ simulations.

The proportion (1-P) of the genome that evolved under heterogeneous migration in models with parameter $2m$, was 0.26, meaning that almost one third of the genome is subject to constrained gene flow because of barrier loci. The effective population sizes of the daughter populations $Nu1$ and $Nu2$, indicate a severe bottleneck in the populations ($b1$ and $b2 < 1$) since the time of population split. The local effect of selection at linked sites seems to affect only 20% of loci ($Q = 0.17$) with a relatively large value of hrf (Hill-Roberston factor = ~ 0.14) (Table 3). Meanwhile, the proportion of the genome that evolved under heterogeneous migration in models with parameter $2m$ between north and south, was 0.97, meaning that the majority of the genome is subject to constrained gene flow because of barrier loci. The local effect of selection at linked sites seems to affect almost half of the loci ($Q = 0.49$) with a relatively large value of hrf (Hill-Roberston factor = ~ 0.11) (Table 3).

Both comparisons depict asymmetrical migration rate northward, with $5.97 (m_{21}) > 0.68 (m_{12})$ for Mid-North and $4.64 (m_{12}) > 1.03 (m_{21})$ for North-South (table 3). The number of migrants (estimated by $(N1*b1*m_{12})/2$ and $(N2*b2*m_{21})/2$) between the north and mid (1=mid & 2=north) is asymmetrical, and predominantly (albeit weakly) northward oriented with ($Nm_{north \leftarrow mid} = 0.25$) than in the opposite direction ($Nm_{mid \leftarrow north} = 0.12$). Nme was used to explain the orientation of gene flow between north and south as this parameter was highly asymmetrical while Nm was very similar between the two

populations (Table 3). Gene flow was predominantly northward oriented between the two populations as captured by N_{me} ($N_{me_{north < south}} = 2.40$, $N_{me_{south < north}} = 0.66$). In this case, N_{me} does not represent true migrants, but rather the movement of introgressed alleles that are not impacted by barrier loci.

3.6 Effective Population Size (N_e)

Contemporary N_e estimates using parameters from $\partial a \partial i$ were high. When comparing the north and mid populations, N_e was calculated as 299,738 and 202,206 for the north and mid, respectively, showing a sharp decrease in N_e from an N_{anc} of 401,202 since the $T_{div} \sim 123$ kya. When comparing the north and south, N_e was calculated as 701,645 and 865,000 for the north and south, respectively, indicating an increase in N_e from an N_{anc} of 677,263 since the $T_{div} \sim 335$ kya. Nevertheless, it remains complicated to distinguish the differences between a decrease in the effective population size caused by a severe bottleneck, as this signature in structured populations can also be caused by a reduction of the gene flow over time, and these results are therefore interpreted with caution.

3.7 Suitability of larval dispersal models in predicting empirical patterns of gene flow in genomic datasets

3.7.1 Larval dispersal models

Larval dispersal probability models were run with a passive vertical migration parameter, a growth curve for copepods based on temperature response, and millions of particles released daily from 2010-2016. Particles dispersed predominantly northward, particularly in the case of the mid and south vent fields. Particles dispersing from the

north dispersed further east and west than the other sites. Larval dispersal from the south and mid was constrained by the topography around the Peggy Ridge and the presence of the Niuafu'ou plate. The lowest pairwise probability of dispersal among vent fields was 7.25⁻³² from ABE to Mangatolo (northward), while the highest was 3.26⁻⁷ from Tui Malila to ABE (northward) (figure 6A). Despite the low probability values, all vent fields were connected to one another by very limited dispersal (values above 0) except the north (figure 6B), and all vent fields displayed high levels of self-recruitment, highest so in the mid and south. The average LDD of Lagrangian particles dispersing from all vent fields was ~104 days (S10, figure 11).

3.7.2 Migration inferred from genomic data

Using empirical allele frequency data, *DivMigrate* identified significant, asymmetric, northward migration from the southern and mid populations to the north (Figure 6A). From the south to the north, *Nm* was 1.0 per generation, describing unidirectional gene flow in purely northward orientation. From the mid to the north, *Nm* was 0.31 indicative of a weaker, northward gene flow. From the mid to the south, *Nm* was 0.33, indicative of a weak, southward gene flow (Figure 6A). These values were calculated under the strong assumption of a n-islands model with no demographic changes, however, results from *DivMigrate* are comparable to those from $\partial a \partial i$, with strong northward, asymmetric gene flow, and approximately one third of each generation of migrants emigrating from the mid to the north, and over twice the amount of migrants per generation emigrating from the south to the north.

3.8 Genotype-Environment Association Analysis

A db-RDA conducted on a subset of 671 SNPs significantly associated with environmental variables revealed that structural variables of intermediate scales (MEM4 and MEM5) appeared to correlate significantly with differences between Tahi and ABE on one hand, and Tui Malila and Mangatolo, on the other hand (S8, figure 8, table 3). An AEM defining high probabilities of dispersal (AEM1) also appeared to correlate significantly with differences between these two groups of populations. The RDA had a global R^2 value of 0.84 (p -value <0.001). MEM5, MEM4, and AEM1 were highly significant with p -values of <0.001 for all parameters. RDA1, explaining 83.78 % of the genomic variation was also highly significant with a p -value of <0.001 , while RDA2 explained 3.21 % of the variation (p -value = <0.001).

4. Discussion

This study examines population connectivity of the copepod *S. lauensis* in the Lau basin, a hydrothermal vent habitat in the Southwest Pacific BABs. Using 5,778 SNPs, we confirmed strong spatial and temporal structuring, with metapopulations originating from three ancestral pools. Population separation likely occurred around ~119 kya (north-mid) and ~326 kya (north-south), with secondary contacts at ~4 kya and ~10 kya, respectively. Weak migration is observed from mid to north and south, while stronger northward migration occurs from south to north. Bespoke larval dispersal patterns captured similar directionality in the gene flow with the exception of gene flow from the mid to the south and supported high levels of structure among all populations.

4.1 Fine-scale population structure

Previous studies have shown that within-basin structure is unlikely for megafaunal species with planktonic larval dispersal, except for *Munidopsis lauensis* in the Manus basin (Mitarai et al., 2016; Plouviez et al., 2019; Breusing et al., 2021; Tran Lu Y et al., 2021; Poitrimol et al., 2022; Thaler et al., 2014). Although habitat preference and interspecific dynamics are known to influence connectivity patterns (Micheli et al., 2002; Lenihan et al., 2008; Beinart et al., 2012; Johnson et al., 2020), *S. lauensis* experiences high levels of self-recruitment due to its short generation time, reducing the number of migrants being exchanged between populations, thus allowing populations to diverge faster through genetic drift in the absence of migration. Particularly in areas of diffuse hydrothermal venting where *S. lauensis* dominates, nauplii will have less chance of being entrained in a plume vortex and dispersed far into the water column as they are not in close proximity to the vent source. Pronounced geographic structure was evident from ADMIXTURE, IBS, and multiple dimension-reducing techniques within this study.

Temporal genetic structure has been reported for copepods in surface waters resulting from demogenetic changes, due to variations in environmental conditions over time (Tepper and Bradley, 1989; Posavi et al., 2014; Brennan et al., 2022). In the present study, such temporal variations were also depicted at the ABE vent field, as seen in the IBS analysis (S7, figure 7). Allelic introgression from Tu'i Malila (as observed from the ADMIXTURE results in Figure 2B) point to Tu'i Malila having acted as a source for most Lau basin populations after 2016. Furthermore, tectonic rearrangements occurred between 2016 and 2019 with the extinction of the site Kilo Moana which was closer to ABE than Tui' Malila is. However, as the effects of genetic drift act more strongly on small populations due to founder effects, it is also possible that a disruption to the ABE field

caused a sporadic bottleneck. This is supported by the reduction in heterozygosity from 0.12 to 0.08 in samples from ABE from 2016 to 2019. A generation time of 33 generations/year, as reported by Gollner et al. (2016) for copepods at 20°C, was also used, reflecting the r-strategy mechanisms displayed by hydrothermal vent fauna in response to the environmental instability of the vent habitat (O'Connor et al., 2007; Tran Lu Y et al., 2021). Drift acting on a population of reduced size would be especially non-negligible if dirivultid copepods are undergoing 33 generations per year, allowing drift to act on a turnover of almost 100 generations in three years. Bottlenecks also appear to have occurred during the secondary contact event between the north and south, as shown by a decrease in the b1 parameter from the $\partial a \partial i$ results (Table 3). Disruptions to the sea floor of the Lau Basin are evident after the recent Tonga eruption blanketed a large proportion of the Lau Basin, affecting vast areas of seafloor, including ABE (Seabrook et al., 2023). There is evidence of catastrophic eruptions around the Tonga region throughout the last thousand years (Monzier et al., 1994; Lavigne et al., 2021; Brenna et al., 2022), and this activity has increased over the entire Tonga-Kermadec region within this period of time (Watt et al., 2013), indicating that significant changes to the seafloor may have occurred, giving rise to recurrent bottlenecks in populations of benthic organisms.

4.2 Demogenetic history of *S. lauensis* within the Lau basin

The demogenetic history of *S. lauensis* was investigated between the southern, mid, and northern populations of the basin. A mutation rate of 1×10^{-9} , based on relatively recent reports for crustaceans including copepods and amphipods (Thomas et al., 2020), was used to estimate the time of divergence between the populations. This rate is lower than

the typical rate for mitochondrial DNA and aligns with evolutionary rates between mitochondrial and nuclear genomes.

The commencement of spreading in the Mangatolo Triple Junction (MTJ) is estimated to have occurred between 180 and 600 kya (Mensing et al., 2020, Steward et al., 2022), and the birth of the major transform fault, Peggy Ridge, that separates the Australian plate and the Niuafo'ou plate is estimated to be no older than 350 kya (Stewart et al. 2022). The latter appears to act as a major barrier to dispersal at depths below 600 m, and consistently, the time of split between metapopulations is estimated to have occurred after the formation of this fault (327 kya and 119 kya for the north-mid and north-south, respectively). Time of secondary contact events (~4 kya and 10 kya for the north-mid and north-south, respectively) align with *Cox1* data from the same species and vents in the region (Diaz-Recio Lorenzo et al., 2023), that point to an increase in effective population size starting at 10 kya in the Lau basin. During this period, eruptions within the Tonga-Kermadec arc went from making up 10 % of the global eruptions to 50 %, likely giving rise to new vents across the region, and thus more stepping stone features along which dispersal could have occurred (Watt et al., 2013). This would be consistent with the occurrence of an SC event with sufficient genetic exchanges to cause a mixing of *cox1* haplotypes from different geographic regions as reported by Diaz-Recio Lorenzo et al. (2023), while genetic incompatibilities display a pronounced barrier with limited gene flow over a non-negligible portion of the nuclear genome due to a long period of isolation. Despite the rather high standard deviation values of theta for the north-mid (theta = 91.82, SD = 23.55) and the north-south (theta = 155.82, SD = 93.6), demogenetic connectivity patterns appear to be roughly consistent with seabed changes over

geological timescales and the more nuanced events that recently contributed to the complex geological setting of the Lau basin (Ruellan 2003; Martinez and Taylor, 2006; Baker et al., 2019; Baxter et al., 2020). However, stochastic hydrodynamic events such as deep-sea eddies (Speer and Thunher et al., 2012), which may modulate dispersal sporadically alongside significant El Nino events, and modifications to regional surface and deep ocean currents due to the onset of the Last Glacial Maximum, may also have played a role (Hu and Piotrowski et al., 2020, Tran Lu Y et al., 2021). The values used in this study are estimates and should therefore be interpreted cautiously. Assumptions were made regarding generation turnover and non-overlapping generations and may not have fully captured the complex reproductive and dispersal mode of *S. lauensis*. Further research on female fecundity, ecology, and stressors is needed to validate these assumptions for this specific species and the dirivultid family, in general.

4.2.1 Estimation of Effective Population Size (N_e)

An overestimation of N_e can be expected when there is immigration from populations with limited differentiation to the focal population, resulting in less drift due to the increase in alleles introduced that are already present in the population (Nadachowska-Brzyska et al., 2021). Conversely, we expect N_e to be underestimated when structured populations exhibit migrants, introducing foreign alleles, leaving signatures in the genome that resemble genetic drift, which could be the case for *S. lauensis*. Based on the structure analysis it appears that individuals from ABE and Mangatolo from 2019 are admixed with individuals from Tu'i Malila from 2016, which increase temporal variations in these two

populations and would add to the effect of drift in the structured populations, and yet the estimates using $\partial a \partial i$ were high with values ranging from 192,576- 512,415. However, this may also be a result of pooling the two temporal states with use in $\partial a \partial i$, and results of N_e must therefore be interpreted with caution.

4.3 Suitability of larval dispersal models in predicting empirical patterns of gene flow in genomic datasets

Larval dispersal models tested two main hypotheses: depth restriction to the spatial distribution of larvae and gene flow orientation across the Lau basin. The models incorporated realistic scenarios of potential vertical movement and temperature-dependent growth, considering the complex current dynamics within the Lau basin (Speer and Thunherr, 2012; Simons et al., 2021) and the relationship between LDD and temperature (O’Conner et al., 2007). The average larval dispersal duration was estimated to be around 104 days, but potentially with a much shorter duration for self-recruiting copepods in the local vent environment due to high temperatures.

The hypothesis that copepod nauplii travel over short distances with deep-water hydrothermal plumes was confirmed by genetic differentiation of the *cox1* gene of populations among basins (Diaz-Recio Lorenzo et al., 2023) and larval dispersal simulations which showed that particles began leaving the Lau basin from each vent at depths of 600 m and shallower. The simulations indicated highly structured populations, even with a long larval dispersal duration of 104 days. Given the low level of gene flow inferred from the genomic data, it appears that few migrants may be able to travel for a

prolonged period of time, likely in a state of delayed metamorphosis, acting as weak connections between populations. Vertical passive movement allowed particles to cross the transform fault separating the Australian plate and the Niuafo'ou plate, enabling low-level gene flow. However, southward migration probabilities from the mid to the south were zero, despite weak gene flow observed in genomic analyses. Nevertheless, connections may also occur due to stepping-stones and ghost populations aided by the many other vents that exist in the basin (denoted by the white triangles in figure 1) and seafloor fissures forming potential connectivity corridors aided potentially by bottom currents and sub-surface hydrothermal flow, elements not accounted for in the models.

This study identified the mid population, as a contemporary source in 2016, contributing migrants to the north and south. Vents flanking the mid population, including Tow Cam and Kilo Moana, form a cluster facilitating bidirectional gene flow. Tu'i Malila in the south serves as an important source population for northward migration in 2019, however historical changes in the distribution of source populations due to tectonic and volcanic events may have influenced population structure through time. These findings emphasize the significance of these populations in maintaining gene flow towards the north which appears to act as a sink, and highlight the need to consider them in conservation strategies, however they also highlight the need to incorporate time series data, as populations may act as source or sinks depending on the sampling year. While acknowledging the limitations of larval dispersal models, this study demonstrates their value in understanding complex dispersal dynamics by incorporating organism-specific traits.

783 The results of the GEAA analysis showed that intermediate-scale bathymetric structures
784 and fine-scale asymmetric dispersal played a role in structuring *S. lauensis* populations.
785 MEM4, MEM5 (intermediate scale db-MEMs associated with the spatial arrangement of
786 vents), and AEM1 (a fine scale asymmetric vector describing high probabilities of
787 dispersal predicted by Lagrangian simulations) correlated significantly with the observed
788 differences in genotypic frequencies between populations (S8, figure 8, table 3). The db-
789 MEMs used in the analysis likely captured geological features such as vent density,
790 transform faults, depth gradients, and axial ridges in the Lau basin. MEM5 was associated
791 mostly with values of depth, while MEM4 was associated with values of spreading rate.
792 Despite only having one value per vent for depth and spreading rate, these associations
793 appear meaningful, given the depth gradient between Tu'i Malila, ABE, and Tahi Moana
794 (1888 m, 2155 m, and 2273 m, respectively). Meanwhile, the AEM1 was associated with
795 high probabilities of dispersal, suggesting a higher probability of dispersal between the
796 north-south, compared to the mid-south and the mid-north. Depth may play an important
797 role in structuring vent populations, as nauplii from similarly deep vents, would need to
798 cross a smaller depth gradient in order to disperse (Breusing et al., 2021). Spreading rate
799 is an important factor governing both local extinction rate and the rugosity of the seabed
800 (faults and screes) at each vent location. The differences in spreading rates between the
801 north (38 mm/year⁻¹), mid (69mm/year⁻¹), and south (48 mm/year⁻¹) may result in
802 differences in local vent conditions and bacterial communities on which the copepods
803 feed, likely exerting differences among populations, via local adaptation and recurrent
804 bottlenecks. Furthermore, the frequency of vent occurrence is positively correlated with
805 magmatic supply (Baker and German, 2004), which increases with spreading rate (Olive
806 and Dublanchet et al., 2020) implying that fast spreading zones may harbor dense

aggregations of vent sites, providing stepping-stones for copepods to disperse, a theory evaluated for megafauna of the Southwest Pacific vents (Breusing et al., 2021) and also the East Pacific Rise (Jollivet et al., 1999; Vrijenhoek et al., 2010). To the north of ABE and Tahiti Moana, spreading rates increase dramatically from 69 mm/ year⁻¹ to 120 mm/ year⁻¹ (Stewart et al., 2022), as do the number of confirmed vents along that gradient. The aggregations can be seen in e.g., figure 1, where the white triangles denoting known vents appear to form hotspots in the northeast, northwest, and mid/south of the basin. These vents form two main stepping-stone corridors along which vent fauna are distributed, one of which could explain preferential dispersal between north-south, but not between north-mid.

4.4 Connectivity of hydrothermal vent meiofauna vs megafauna – implications for resilience to deep-sea mining

Relative migration inferred from empirical genetic data, agrees largely with that of Breusing et al., (2021), who show that populations of *Alviniconcha* snails exhibit a predominantly southward migration from Tahiti Moana to Tu'i Malila, and a predominantly northward migration from both of those sites to the north. Plouviez et al., (2019) depicted some population structure for the limpet *Lepetodrilus schrolli* using the *cox1* gene and Poitrimol et al. (2022) showed that cryptic species also exist for a range of megafauna in the Southwest Pacific including within the Lau basin based on *cox1*. However, Breusing et al.'s study as well as other recent population genomics studies (Plouviez et al., 2019; Tran Lu Y et al., 2021) and larval dispersal modelling of megafauna in the region (Mitarai et al., 2016) have found little to no structure in the populations within the Lau basin when using

nuclear markers. Our results highlight that pattern of connectivity cannot be generalized to all fauna in vent systems and that the different faunal groups need to be considered when developing robust area-based management tools (ABMTs). The removal of these abundant copepods from the vent environment through mining may have unprecedented consequences for the ecosystem as a whole. Being the most abundant animal where hard substrate is available, dirivultid copepods represent an unexplored but potentially important functional group in these systems, feeding predominantly on chemoautotrophic bacteria (Nomaki et al., 2023) and forming close associations with a range of megafaunal species including *Rimicaris* shrimp (Gollner et al., 2016), the squat lobster *Shinkai crosnieri* (Senokuchi et al., 2018), Bathymodiolin mussels (Gollner 2016), *Ifremeria* and *Alviniconcha* snails (Gollner et al., 2016) and the vent polychaete *Paralvinella sulfincola*, which was hypothesized to utilize the vent copepod *Stygiopontius quadrispinosus* as a primary food source when densities of the copepod were high (1852 ind. per worm) (Limen et al., 2008). Copepods in the global oceans are hugely important bioindicators, and the role of deep-sea copepods at hydrothermal vents as such is largely unexplored. Further research is needed to investigate the trophic role of this family in the vent environment and the potential risks to the ecosystem should populations of abundant copepods suffer major bottlenecks as a result of anthropogenic disturbance.

5. Conclusions

This study reports the first data on population connectivity in the vent meiofauna, specifically for the vent obligate copepod *Stygiopontius lauensis*. Limited gene flow between north and south populations suggests a potential stepping-stone dispersal model

and recent secondary contact events associated with vent dynamics. Divergence between populations likely occurred hundreds of thousands of years ago, with secondary contact events occurring in recent geological history. Our results suggest that migration between vents in the Lau basin is not sufficiently high to offset the effects of drift or local selection, likely leaving populations at risk of local extinction, should mining occur. Larval dispersal models incorporating temperature-dependent dispersal duration and passive vertical movement accurately captured population isolation. However, they did not fully explain the observed low-level southward gene flow from populations in the mid and south, and further research is needed to address this discrepancy. We note that despite the weaknesses in using any single analysis alone to draw conclusions about resilience of vent communities, a multifaceted approach combining multiple complementary analyses provides a much more robust picture of the consequences of anthropogenic activity in these ecosystems. These results add much needed data to connectivity studies in the region, informing dispersal models in the framework of understanding populations at risk of extinction, and shed light on a majorly understudied subgroup of organisms in the Southwest Pacific BAB system.

Acknowledgements

We warmly thank the crew of L'Atalante, the scientific members of the cruise who sorted the copepod samples (Camille Poitrimol and Eve-Julie Arsenault-Pernet) and the chief scientists of the Chubacarc cruise (Didier Jollivet and Stéphane Hourdez) for kindly donating the 2019 samples. We also warmly thank Roxanne Beinart, chief scientist, for the donation of the samples collected during the 2016 FK160407 cruise and ABIMS Bioinformatics platform of the Station Biologique de Roscoff (France) which provided

computing resources for the demographic analysis. Ship time was supported by the French Oceanographic Fleet programme (CHUBACARC cruise <https://doi.org/10.17600/18001111> to Didier Jollivet and Stephane Hourdez), INEE (CNRS) and the Agence Nationale de la Recherche (ANR) that funded the project “CERBERUS” (contract number ANR-17CE02-0003 to Stephane Hourdez). Sequencing was funded by the UU-NIOZ under the project “Protecting deep-seabed hydrothermal vents via area-based management tools” (to Sabine Gollner). We would also like to thank the two anonymous reviewers for their suggestions and comments to improve the manuscript

Data availability

Raw sequence reads (Individual fasta files), individual genotype data (VCF) and metadata are available on DataDryad (<https://doi.org/10.5061/dryad.zkh1893g2>). Scripts used in this study (R, *ada*) are available on a public Github repositories: <https://github.com/Atranluy/Scripts-Ifremeria>, <https://github.com/otistwo/hydrothermal-thesis/blob/main/PARCELS/Copepod-PARC-ELS.ipynb>, and <https://github.com/otistwo/hydrothermal-thesis/blob/main/PARCELS/Copepod-post-hoc.ipynb>.

4. Bibliography

- Alexander, D.H., Lange, K., 2011a. Enhancements to the ADMIXTURE algorithm for individual ancestry estimation. BMC Bioinformatics 12, 246. <https://doi.org/10.1186/1471-2105-12-246>
- Araneda, C., Larraín, M.A., Hecht, B. and Narum, S., 2016. Adaptive genetic variation distinguishes Chilean blue mussels (*Mytilus chilensis*) from different marine environments. Ecol Evol. 6: 3632-3644. <https://doi.org/10.1002/ece3.2110>
- Baker, E.T., German, C.R., 2013. On the Global Distribution of Hydrothermal Vent Fields, in: German, C.R., Lin, J., Parson, L.M. (Eds.), Geophysical Monograph Series.

- American Geophysical Union, Washington, D. C., pp. 245–266.
<https://doi.org/10.1029/148GM10>
- Baker, E.T., Walker, S.L., Massoth, G.J., Resing, J.A., 2019. The NE Lau Basin: Widespread and Abundant Hydrothermal Venting in the Back-Arc Region Behind a Superfast Subduction Zone. *Front. Mar. Sci.* 6, 382.
<https://doi.org/10.3389/fmars.2019.00382>
- Bashevkin, S.M., Dibble, C.D., Dunn, R.P., Hollarsmith, J.A., Ng, G., Satterthwaite, E.V., Morgan, S.G., 2020. Larval dispersal in a changing ocean with an emphasis on upwelling regions. *Ecosphere* 11. <https://doi.org/10.1002/ecs2.3015>
- Beedessee, G., Watanabe, H., Ogura, T., Nemoto, S., Yahagi, T., Nakagawa, S., Nakamura, K., Takai, K., Koonjul, M., Marie, D.E.P., 2013. High Connectivity of Animal Populations in Deep-Sea Hydrothermal Vent Fields in the Central Indian Ridge Relevant to Its Geological Setting. *PLoS ONE* 8, e81570.
<https://doi.org/10.1371/journal.pone.0081570>
- Beinart, R.A., Sanders, J.G., Faure, B., Sylva, S.P., Lee, R.W., Becker, E.L., Gartman, A., Luther, G.W., Seewald, J.S., Fisher, C.R., Girguis, P.R., 2012. Evidence for the role of endosymbionts in regional-scale habitat partitioning by hydrothermal vent symbioses. *Proc. Natl. Acad. Sci. U.S.A.* 109.
<https://doi.org/10.1073/pnas.1202690109>
- Benestan, L., Quinn, B.K., Maaroufi, H., Laporte, M., Clark, F.K., Greenwood, S.J., Rochette, R., Bernatchez, L., 2016. Seascape genomics provides evidence for thermal adaptation and current-mediated population structure in American lobster (*Homarus americanus*). *Mol Ecol* 25, 5073–5092.
<https://doi.org/10.1111/mec.13811>
- Benestan, L.M., Ferchaud, A., Hohenlohe, P.A., Garner, B.A., Naylor, G.J.P., Baums, I.B., Schwartz, M.K., Kelley, J.L., Luikart, G., 2016. Conservation genomics of natural and managed populations: building a conceptual and practical framework. *Molecular Ecology* 25, 2967–2977. <https://doi.org/10.1111/mec.13647>
- Benestan, L.M., Rougemont, Q., Senay, C., Normandeau, E., Parent, E., Rideout, R., Bernatchez, L., Lambert, Y., Audet, C., Parent, G.J., 2021. Population genomics and history of speciation reveal fishery management gaps in two related redfish species (*Sebastes mentella* and *Sebastes fasciatus*). *Evol Appl* 14, 588–606.
<https://doi.org/10.1111/eva.13143>
- Bernatchez, S., Xuereb, A., Laporte, M., Benestan, L., Steeves, R., Laflamme, M., Bernatchez, L., Mallet, M.A., 2019. Seascape genomics of eastern oyster (*Crassostrea virginica*) along the Atlantic coast of Canada. *Evol Appl* 12, 587–609. <https://doi.org/10.1111/eva.12741>

- Blanchard, C., Gollner, S., 2022. Area-based management tools to protect unique hydrothermal vents from harmful effects from deep-sea mining: A review of ongoing developments. *Front. Polit. Sci.* 4, 1033251. <https://doi.org/10.3389/fpos.2022.1033251>
- Blasiak, R., Wynberg, R., Grorud-Colvert, K., Thambisetty, S., Bandarra, N.M., Canário, A.V.M., Da Silva, J., Duarte, C.M., Jaspars, M., Rogers, A., Sink, K., Wabnitz, C.C.C., 2020. The ocean genome and future prospects for conservation and equity. *Nat Sustain* 3, 588–596. <https://doi.org/10.1038/s41893-020-0522-9>
- Brenna, M., Cronin, S. J., Smith, I. E. M., Pntesilli, A., Tost, M., Barker, S. J., Tonga'onevai, S., Kula, T., Vaiomounga R., 2022. Post-caldera volcanism reveals shallow priming of an intra-ocean arc andesitic caldera: Hunga volcano, Tonga, SW Pacific. *Lithos* 412–413. *Lithos* 412–413. <https://doi.org/10.1016/j.lithos.2022.106614>
- Brennan, R.S., deMayo, J.A., Dam, H.G., Finiguerra, M., Baumann, H., Buffalo, V., Pespeni, M.H., 2022a. Experimental evolution reveals the synergistic genomic mechanisms of adaptation to ocean warming and acidification in a marine copepod. *Proc. Natl. Acad. Sci. U.S.A.* 119, e2201521119. <https://doi.org/10.1073/pnas.2201521119>
- Brennan, R.S., deMayo, J.A., Dam, H.G., Finiguerra, M., Baumann, H., Buffalo, V., Pespeni, M.H., 2022b. Experimental evolution reveals the synergistic genomic mechanisms of adaptation to ocean warming and acidification in a marine copepod. *Proc. Natl. Acad. Sci. U.S.A.* 119, e2201521119. <https://doi.org/10.1073/pnas.2201521119>
- Breusing, C., Biastoch, A., Drews, A., Metaxas, A., Jollivet, D., Vrijenhoek, R.C., Bayer, T., Melzner, F., Sayavedra, L., Petersen, J.M., Dubilier, N., Schilhabel, M.B., Rosenstiel, P., Reusch, T.B.H., 2016. Biophysical and Population Genetic Models Predict the Presence of “Phantom” Stepping Stones Connecting Mid-Atlantic Ridge Vent Ecosystems. *Current Biology* 26, 2257–2267. <https://doi.org/10.1016/j.cub.2016.06.062>
- Breusing, C., Johnson, S.B., Mitarai, S., Beinart, R.A., Tunnicliffe, V., 2023. Differential patterns of connectivity in Western Pacific hydrothermal vent metapopulations: A comparison of biophysical and genetic models. *Evolutionary Applications* 16, 22–35. <https://doi.org/10.1111/eva.13326>
- Breusing, C., Johnson, S.B., Tunnicliffe, V., Vrijenhoek, R.C., 2015. Population structure and connectivity in Indo-Pacific deep-sea mussels of the *Bathymodiolus septemdierum* complex. *Conserv Genet* 16, 1415–1430. <https://doi.org/10.1007/s10592-015-0750-0>
- Brunner, O., Methou, P., Mitarai, S., 2023. The Role of Reproductive Periodicity in Dispersal Among Hydrothermal Vents and its Implications for Regional

Connectivity and Conservation (preprint). Biophysics.
<https://doi.org/10.1101/2023.03.07.531641>

Casanova, A., Maroso, F., Blanco, A., Hermida, M., Ríos, N., García, G., Manuzzi, A., Zane, L., Verissimo, A., García-Marín, J.-L., Bouza, C., Vera, M., Martínez, P., 2021. Low impact of different SNP panels from two building-loci pipelines on RAD-Seq population genomic metrics: case study on five diverse aquatic species. BMC Genomics 22, 150. <https://doi.org/10.1186/s12864-021-07465-w>

Fisher C. R., and Girguis P., 2016. cruise doi: <https://doi.org/10.7284/906664>

Chattopadhyay, B., Garg, K.M., Ramakrishnan, U., 2014. Effect of diversity and missing data on genetic assignment with RAD-Seq markers. BMC Res Notes 7, 841. <https://doi.org/10.1186/1756-0500-7-841>

Craddock, C., Hoeh, W.R., Gustafson, R.G., Lutz, R.A., Hashimoto, J., Vrijenhoek, R.J., 1995. Evolutionary relationships among deep-sea mytilids (Bivalvia: Mytilidae) from hydrothermal vents and cold-water methane/sulfide seeps. Marine Biology 121, 477–485. <https://doi.org/10.1007/BF00349456>

Crotti, M., Barratt, C.D., Loader, S.P., Gower, D.J., Streicher, J.W., 2019. Causes and analytical impacts of missing data in RADseq phylogenetics: Insights from an African frog (*Afrixalus*). Zool Scr 48, 157–167. <https://doi.org/10.1111/zsc.12335>

Dalongeville, A., Benestan, L., Mouillot, D., Lobreaux, S., Manel, S., 2018. Combining six genome scan methods to detect candidate genes to salinity in the Mediterranean striped red mullet (*Mullus surmuletus*). BMC Genomics 19, 217. <https://doi.org/10.1186/s12864-018-4579-z>

De Jode, A., Le Moan, A., Johannesson, K., Faria, R., Stankowski, S., Westram, A.M., Butlin, R.K., Rafajlović, M., Fraïsse, C., 2023. Ten years of demographic modelling of divergence and speciation in the sea. Evolutionary Applications 16, 542–559. <https://doi.org/10.1111/eva.13428>

De Wit, P., Faust, E., Green, L., Jahnke, M., Pereyra, R.T., Rafajlović, M., 2023. A decade of progress in marine evolutionary biology. Evolutionary Applications 16, 193–201. <https://doi.org/10.1111/eva.13523>

Delandmeter, P., Van Sebille, E., 2019. The Parcels v2.0 Lagrangian framework: new field interpolation schemes. Geosci. Model Dev. 12, 3571–3584. <https://doi.org/10.5194/gmd-12-3571-2019>

Diaz-Papkovich, A., Anderson-Trocmé, L., Ben-Eghan, C., Gravel, S., 2019. UMAP reveals cryptic population structure and phenotype heterogeneity in large genomic cohorts. PLoS Genet 15, e1008432. <https://doi.org/10.1371/journal.pgen.1008432>

- Diaz-Papkovich, A., Anderson-Trocmé, L., Gravel, S., 2021. A review of UMAP in population genetics. *J Hum Genet* 66, 85–91. <https://doi.org/10.1038/s10038-020-00851-4>
- Diaz-Recio Lorenzo, C., Bruggen, D.T., Luther, G.W., Gartman, A., Gollner, S., 2021a. Copepod assemblages along a hydrothermal stress gradient at diffuse flow habitats within the ABE vent site (Eastern Lau Spreading Center, Southwest Pacific). *Deep Sea Research Part I: Oceanographic Research Papers* 173, 103532. <https://doi.org/10.1016/j.dsr.2021.103532>
- Diaz-Recio Lorenzo, C., Patel, T., Arsenault-Pernet, E.-J., Poitrimol, C., Jollivet, D., Martinez Arbizu, Gollner S., 2023. Highly structured populations of 42 deep-sea copepods associated with hydrothermal vents across the Southwest Pacific, despite contrasting life history traits. *PLoS ONE* 18(11): e0292525. <https://doi.org/10.1371/journal.pone.0292525>
- Do, C., Waples, R.S., Peel, D., Macbeth, G.M., Tillett, B.J. and Ovenden, J.R., 2014. NeEstimator v2: re-implementation of software for the estimation of contemporary effective population size (Ne) from genetic data. *Mol Ecol Res.* 14: 209–214. <https://doi.org/10.1111/1755-0998.12157>
- Dorant, Y., Laporte, M., Rougemont, Q., Cayuela, H., Rochette, R., & Bernatchez, L. (2022). Landscape genomics of the American lobster (*Homarus americanus*). *Molecular Ecology*, 31, 5182– 5200. <https://doi.org/10.1111/mec.16653>
- Dray, S., Péliissier, R., Couteron, P., Fortin, M.-J., Legendre, P., Peres-Neto, P.R., Bellier, E., Bivand, R., Blanchet, F.G., De Cáceres, M., Dufour, A.-B., Heegaard, E., Jombart, T., Munoz, F., Oksanen, J., Thioulouse, J., Wagner, H.H., 2012. Community ecology in the age of multivariate multiscale spatial analysis. *Ecological Monographs* 82, 257–275. <https://doi.org/10.1890/11-1183.1>
- Drazen, J.C., Smith, C.R., Gjerde, K.M., Haddock, S.H.D., Carter, G.S., Choy, C.A., Clark, M.R., Dutrieux, P., Goetze, E., Hauton, C., Hatta, M., Koslow, J.A., Leitner, A.B., Pacini, A., Perelman, J.N., Peacock, T., Sutton, T.T., Watling, L., Yamamoto, H., 2020. Midwater ecosystems must be considered when evaluating environmental risks of deep-sea mining. *Proc. Natl. Acad. Sci. U.S.A.* 117, 17455–17460. <https://doi.org/10.1073/pnas.2011914117>
- Du Preez, C., Fisher, C.R., 2018. Long-Term Stability of Back-Arc Basin Hydrothermal Vents. *Front. Mar. Sci.* 5, 54. <https://doi.org/10.3389/fmars.2018.00054>
- Duruz, S., Sevane, N., Selmoni, O., Vajana, E., Leempoel, K., Stucki, S., Orozco-terWengel, P., Rochat, E., Dunner, S., The NEXTGEN Consortium, The CLIMGEN Consortium, Bruford, M.W., Joost, S., 2019. Rapid identification and interpretation of gene–environment associations using the new R.SamBada landscape genomics

- pipeline. *Mol Ecol Resour* 19, 1355–1365. <https://doi.org/10.1111/1755-0998.13044>
- Eaton, D.A.R., Spriggs, E.L., Park, B., Donoghue, M.J., 2016. Misconceptions on Missing Data in RAD-seq Phylogenetics with a Deep-scale Example from Flowering Plants. *Syst Biol* syw092. <https://doi.org/10.1093/sysbio/syw092>
- Eldon, B., Riquet, F., Yearsley, J., Jollivet, D., Broquet, T., 2016. Current hypotheses to explain genetic chaos under the sea. *Curr Zool* 62, 551–566. <https://doi.org/10.1093/cz/zow094>
- Pereira, E., Mateus, C.S., Alves, M. J., Almeida, R., Pereira, J., Quintella, B. R., Almeida, P. R., 2023. Connectivity patterns and gene flow among Chelon ramada populations. *Estuarine, Coastal and Shelf Science*. 281: 108209, ISSN 0272-7714. <https://doi.org/10.1016/j.ecss.2022.108209>
- Beaumont M. A., Nichols R. A., 1996. Evaluating loci for use in the genetic analysis of population structure, 1996. . *Proc. R. Soc. Lond. B* 263, 1619–1626. <https://doi.org/10.1098/rspb.1996.0237>
- Excoffier, L., Dupanloup, I., Huerta-Sánchez, E., Sousa, V.C., Foll, M., 2013. Robust Demographic Inference from Genomic and SNP Data. *PLoS Genet* 9, e1003905. <https://doi.org/10.1371/journal.pgen.1003905>
- Excoffier, L., Lischer H. E. L., 2010. Arlequin suite ver 3.5: a new series of programs to perform population genetics analyses under Linux and Windows. *Mol. Ecol. Res.* 10(3): 564-567. <https://doi.org/10.1111/j.1755-0998.2010.02847.x>
- Faria, R., Johannesson, K., Stankowski, S., 2021. Speciation in marine environments: Diving under the surface. *J of Evolutionary Biology* 34, 4–15. <https://doi.org/10.1111/jeb.13756>
- Ferrini, V.L., Tivey, M.K., Carbotte, S.M., Martinez, F., Roman, C., 2008. Variable morphologic expression of volcanic, tectonic, and hydrothermal processes at six hydrothermal vent fields in the Lau back-arc basin: Hydrothermal Processes in Lau Back-arc Basin. *Geochem. Geophys. Geosyst.* 9, n/a-n/a. <https://doi.org/10.1029/2008GC002047>
- Foll, M., Gaggiotti, O., 2008. A Genome-Scan Method to Identify Selected Loci Appropriate for Both Dominant and Codominant Markers: A Bayesian Perspective. *Genetics* 180, 977–993. <https://doi.org/10.1534/genetics.108.092221>
- Folmer, O., Black, M., Hoeh, W., Lutz, R., And Vrijenhoek, R., 1994. DNA primers for amplification of mitochondrial cytochrome c oxidase subunit I from diverse metazoan invertebrates. *Molecular Marine Biology and Biotechnology*. 3294-299.

- François, O., Martins, H., Caye, K., Schoville, S.D., 2016. Controlling false discoveries in genome scans for selection. *Mol Ecol* 25, 454–469. <https://doi.org/10.1111/mec.13513>
- Gagnaire, P.-A., Gaggiotti, O.E., 2016. Detecting polygenic selection in marine populations by combining population genomics and quantitative genetics approaches. *Curr Zool* 62, 603–616. <https://doi.org/10.1093/cz/zow088>
- Gartman, A., Yücel, M., Madison, A.S., Chu, D.W., Ma, S., Janzen, C.P., Becker, E.L., Beinart, R.A., Girguis, P.R., Luther, G.W., 2011. Sulfide Oxidation across Diffuse Flow Zones of Hydrothermal Vents. *Aquat Geochem* 17, 583–601. <https://doi.org/10.1007/s10498-011-9136-1>
- Gauthier, J., Mouden, C., Suchan, T., Alvarez, N., Arrigo, N., Riou, C., Lemaitre, C., Peterlongo, P., 2020. DiscoSnp-RAD: de novo detection of small variants for RAD-Seq population genomics. *PeerJ* 8, e9291. <https://doi.org/10.7717/peerj.9291>
- Gautier, M., Foucaud, J., Gharbi, K., Cézard, T., Galan, M., Loiseau, A., Thomson, M., Pudlo, P., Kerdelhué, C., Estoup, A., 2013. Estimation of population allele frequencies from next-generation sequencing data: pool-versus individual-based genotyping. *Mol Ecol* 22, 3766–3779. <https://doi.org/10.1111/mec.12360>
- Gollner, S., Fontaneto, D., Martínez Arbizu, P., 2011. Molecular taxonomy confirms morphological classification of deep-sea hydrothermal vent copepods (Dirivultidae) and suggests broad physiological tolerance of species and frequent dispersal along ridges. *Mar Biol* 158, 221–231. <https://doi.org/10.1007/s00227-010-1553-y>
- Gollner, S., Govenar, B., Fisher, C., Bright, M., 2015. Size matters at deep-sea hydrothermal vents: different diversity and habitat fidelity patterns of meio- and macrofauna. *Mar. Ecol. Prog. Ser.* 520, 57–66. <https://doi.org/10.3354/meps11078>
- Gollner, S., Govenar, B., Martinez Arbizu, P., Mullineaux, L.S., Mills, S., Le Bris, N., Weinbauer, M., Shank, T.M., Bright, M., 2020. Animal Community Dynamics at Senescent and Active Vents at the 9°N East Pacific Rise After a Volcanic Eruption. *Front. Mar. Sci.* 6, 832. <https://doi.org/10.3389/fmars.2019.00832>
- Gollner, S., Ivanenko, V.N., Arbizu, P.M., Bright, M., 2010. Advances in Taxonomy, Ecology, and Biogeography of Dirivultidae (Copepoda) Associated with Chemosynthetic Environments in the Deep Sea. *PLoS ONE* 5, e9801. <https://doi.org/10.1371/journal.pone.0009801>
- Gollner, S., Kaiser, S., Menzel, L., Jones, D.O.B., Brown, A., Mestre, N.C., Van Oevelen, D., Menot, L., Colaço, A., Canals, M., Cuvelier, D., Durden, J.M., Gebruk, A., Eggho, G.A., Haeckel, M., Marcon, Y., Mevenkamp, L., Morato, T., Pham, C.K., Purser, A.,

- Sanchez-Vidal, A., Vanreusel, A., Vink, A., Martinez Arbizu, P., 2017. Resilience of benthic deep-sea fauna to mining activities. *Marine Environmental Research* 129, 76–101. <https://doi.org/10.1016/j.marenvres.2017.04.010>
- Gollner, S., Stuckas, H., Kihara, T.C., Laurent, S., Kodami, S., Martinez Arbizu, P., 2016. Mitochondrial DNA Analyses Indicate High Diversity, Expansive Population Growth and High Genetic Connectivity of Vent Copepods (Dirivultidae) across Different Oceans. *PLoS ONE* 11, e0163776. <https://doi.org/10.1371/journal.pone.0163776>
- Gutenkunst, R.N., Hernandez, R.D., Williamson, S.H., Bustamante, C.D., 2009. Inferring the Joint Demographic History of Multiple Populations from Multidimensional SNP Frequency Data. *PLoS Genet* 5, e1000695. <https://doi.org/10.1371/journal.pgen.1000695>
- Hey, R.N., Massoth, G.J., Vrijenhoek, R.C., Rona, P.A., Lupton, J., Butterfield, D.A., 2006. Hydrothermal Vent Geology and Biology at Earth's Fastest Spreading Rates. *Mar Geophys Res* 27, 137–153. <https://doi.org/10.1007/s11001-005-1887-x>
- Holderegger, R., Wagner, H.H., 2006. A brief guide to Landscape Genetics. *Landscape Ecol* 21, 793–796. <https://doi.org/10.1007/s10980-005-6058-6>
- Honza, E., 1995. Spreading mode of backarc basins in the western Pacific. *Tectonophysics* 251, 139–152. [https://doi.org/10.1016/0040-1951\(95\)00054-2](https://doi.org/10.1016/0040-1951(95)00054-2)
- Hourdez S. And Jollivet D (2019) CHUBACARC cruise, RV L'Atalante. <https://doi.org/10.17600/18001111>
- Hourdez, S., Jollivet, D., 2020. Metazoan adaptation to deep-sea hydrothermal vents, in: Di Prisco, G., Edwards, H.G.M., Elster, J., Huiskes, A.H.L. (Eds.), *Life in Extreme Environments*. Cambridge University Press, pp. 42–67. <https://doi.org/10.1017/9781108683319.004>
- Hu, E.-Z., Lan, X.-R., Liu, Z.-L., Gao, J., Niu, D.-K., 2022. A positive correlation between GC content and growth temperature in prokaryotes. *BMC Genomics* 23, 110. <https://doi.org/10.1186/s12864-022-08353-7>
- Hu, R., Piotrowski, A.M., 2018. Neodymium isotope evidence for glacial-interglacial variability of deepwater transit time in the Pacific Ocean. *Nat Commun* 9, 4709. <https://doi.org/10.1038/s41467-018-07079-z>
- Hurtado, L.A., Lutz, R.A., Vrijenhoek, R.C., 2004. Distinct patterns of genetic differentiation among annelids of eastern Pacific hydrothermal vents. *Mol Ecol* 13, 2603–2615. <https://doi.org/10.1111/j.1365-294X.2004.02287.x>

- Ingels, J., Leduc, D., Zeppilli, D., Vanreusel, A., 2023. Deep-Sea Meiofauna—A World on Its Own or Deeply Connected? In: Giere, O., Schratzberger, M. (eds) *New Horizons in Meiobenthos Research*. Springer, Cham.
https://doi.org/10.1007/978-3-031-21622-0_8
- Ivanenko, V.N., Martínez Arbizu, P., Stecher, J., 2007. Lecithotrophic nauplius of the family Dirivultidae (Copepoda; Siphonostomatoida) hatched on board over the Mid-Atlantic Ridge (5°S): Nauplius of Dirivultidae (Copepoda). *Marine Ecology* 28, 49–53. <https://doi.org/10.1111/j.1439-0485.2007.00142.x>
- John, C.R., Watson, D., Russ, D., Goldmann, K., Ehrenstein, M., Pitzalis, C., Lewis, M., Barnes, M., 2020. M3C: Monte Carlo reference-based consensus clustering. *Sci Rep* 10, 1816. <https://doi.org/10.1038/s41598-020-58766-1>
- Johnson, S.B., Warén, A., Tunnicliffe, V., Dover, C.V., Wheat, C.G., Schultz, T.F., Vrijenhoek, R.C., 2015. Molecular taxonomy and naming of five cryptic species of *Alviniconcha* snails (Gastropoda: Abysochrysoidea) from hydrothermal vents. *Systematics and Biodiversity* 13, 278–295.
<https://doi.org/10.1080/14772000.2014.970673>
- Jollivet, D., Chevaldonné, P., Planque, B., 1999. Polychaete dispersal in the eastern pacific. 2. A metapopulation model based on habitat shifts. *Evolution*. 53(4): 1128–1141. <https://doi.org/10.1111/j.1558-5646.1999.tb04527.x>
- Jollivet, D., Desbruyères, D., Bonhomme, F., Moraga, D., 1995. Genetic differentiation of deep-sea hydrothermal vent alvinellid populations (Annelida: Polychaeta) along the East Pacific Rise. *Heredity* 74, 376–391.
<https://doi.org/10.1038/hdy.1995.56>
- Kakee, T., 2020. Deep-sea mining legislation in Pacific Island countries: From the perspective of public participation in approval procedures. *Marine Policy* 117, 103881. <https://doi.org/10.1016/j.marpol.2020.103881>
- Keenan, K., McGinnity, P., Cross, T.F., Crozier, W.W., Prodöhl, P.A., 2013. diveRsity : An R package for the estimation and exploration of population genetics parameters and their associated errors. *Methods Ecol Evol* 4, 782–788.
<https://doi.org/10.1111/2041-210X.12067>
- Knaus, B.J., Grünwald, N.J., 2017. VCFR: a package to manipulate and visualize variant call format data in R. *Mol Ecol Res*, 17(1), 44–53. ISSN 757.
<https://dx.doi.org/10.1111/1755-0998.12549>
- Lavigne, F., Morin, J., Wassmer, P., Weller, O., Kula, T., Maea, A. V., Kelfoun, K., Mokadem, F., Paris, R., Malawani, M. N., Farai, A., Benbakkar, M., Saulnier-Copard, S., Vidal, C. M., Tu’I’afitu, T., Kitekei’aho, F., Trautmann, M., Gomez, C., 2021. Bridging Legends and Science: Field Evidence of a Large Tsunami that Affected the

- Kingdom of Tonga in the 15th Century. *Front. Earth. Sci.* 9:748755.
<https://doi.org/10.3389/feart.2021.748755>
- Leaché, A., Ogilvie, H.A., 2016. Bayes Factor Delimitation of Species (*with genomic data; BFD*): A Tutorial and Worked Example.
- Legendre, P., Gauthier, O., 2014. Statistical methods for temporal and space-time analysis of community composition data <sup/>. *Proc. R. Soc. B.* 281, 20132728.
<https://doi.org/10.1098/rspb.2013.2728>
- Lelièvre, Y., Sarrazin, J., Marticorena, J., Schaal, G., Day, T., Legendre, P., Hourdez, S., Matabos, M., 2018. Biodiversity and trophic ecology of hydrothermal vent fauna associated with tubeworm assemblages on the Juan de Fuca Ridge. *Biogeosciences* 15, 2629–2647. <https://doi.org/10.5194/bg-15-2629-2018>
- Lenihan, H.S., Mills, S.W., Mullineaux, L.S., Peterson, C.H., Fisher, C.R., Micheli, F., 2008. Biotic interactions at hydrothermal vents: Recruitment inhibition by the mussel *Bathymodiolus thermophilus*. *Deep Sea Research Part I: Oceanographic Research Papers* 55, 1707–1717. <https://doi.org/10.1016/j.dsr.2008.07.007>
- Levin, L.A., Amon, D.J., Lily, H., 2020. Challenges to the sustainability of deep-seabed mining. *Nat Sustain* 3, 784–794. <https://doi.org/10.1038/s41893-020-0558-x>
- Limén, H., Stevens, C., Bourass, Z., Juniper, S., 2008. Trophic ecology of siphonostomatoid copepods at deep-sea hydrothermal vents in the northeast Pacific. *Mar. Ecol. Prog. Ser.* 359, 161–170.
<https://doi.org/10.3354/meps07344>
- Lotterhos, K.E., Whitlock, M.C., 2015. The relative power of genome scans to detect local adaptation depends on sampling design and statistical method. *Mol Ecol* 24, 1031–1046. <https://doi.org/10.1111/mec.13100>
- Lowry, D.B., Hoban, S., Kelley, J.L., Lotterhos, K.E., Reed, L.K., Antolin, M.F., Storfer, A., 2017. Breaking RAD: an evaluation of the utility of restriction site-associated DNA sequencing for genome scans of adaptation. *Mol Ecol Resour* 17, 142–152.
<https://doi.org/10.1111/1755-0998.12635>
- Luikart, G., England, P.R., Tallmon, D., Jordan, S., Taberlet, P., 2003. The power and promise of population genomics: from genotyping to genome typing. *Nat Rev Genet* 4, 981–994. <https://doi.org/10.1038/nrg1226>
- Luu, K., Bazin, E., Blum, M. G. B., 2017. pcadapt: an R package to perform genome scans for selection based on principal component analysis. *Mol. Ecol. Res.* 17(1): 67-77.
<https://doi.org/10.1111/1755-0998.12592>

- Mackenzie, C.L., Kent, F.E.A., Baxter, J.M., Gormley, K.S.G., Cassidy, A.J., Sanderson, W.G., Porter, J.S., 2022. Genetic Connectivity and Diversity of a Protected, Habitat-Forming Species: Evidence Demonstrating the Need for Wider Environmental Protection and Integration of the Marine Protected Area Network. *Front. Mar. Sci.* 9, 772259. <https://doi.org/10.3389/fmars.2022.772259>
- Martinez, F., Taylor, B., 2006. Modes of crustal accretion in back-arc basins: Inferences from the Lau Basin, in: Christie, D.M., Fisher, C.R., Lee, S.-M., Givens, S. (Eds.), *Geophysical Monograph Series*. American Geophysical Union, Washington, D. C., pp. 5–30. <https://doi.org/10.1029/166GM03>
- Mastretta-Yanes, A., Arrigo, N., Alvarez, N., Jorgensen, T.H., Piñero, D., Emerson, B.C., 2015. Restriction site-associated DNA sequencing, genotyping error estimation and *de novo* assembly optimization for population genetic inference. *Mol Ecol Resour* 15, 28–41. <https://doi.org/10.1111/1755-0998.12291>
- Mees, J., Seys, J., 2023. Book of abstracts – VLIZ Marine Science Day, 1 March 2023, Bruges. Title : VLIZ Special Publication. Vlaams Instituut voor de Zee (VLIZ): Oostende. ISSN 1377-0950 Volume : 90 Issue : Pagination : vi + 112. <https://doi.org/10.48470/41>
- Mensing, R., Stewart, M., Hannington, M., Baxter, A., and Mertmann, D., 2020. The tectonic and volcanic evolution of the Mangatolu Triple Junction, EGU General Assembly 2020, Online, 4–8 May 2020, EGU2020-19897. <https://doi.org/10.5194/egusphere-egu2020-19897>
- Micheli, F., Peterson, C.H., Mullineaux, L.S., Fisher, C.R., Mills, S.W., Sancho, G., Johnson, G.A., Lenihan, H.S., 2002b. PREDATION STRUCTURES COMMUNITIES AT DEEP-SEA HYDROTHERMAL VENTS. *Ecological Monographs* 72, 365–382. [https://doi.org/10.1890/0012-9615\(2002\)072\[0365:PSCADS\]2.0.CO;2](https://doi.org/10.1890/0012-9615(2002)072[0365:PSCADS]2.0.CO;2)
- Milano, I., Babbucci, M., Cariani, A., Atanassova, M., Bekkevold, D., Carvalho, G.R., Espiñeira, M., Fiorentino, F., Garofalo, G., Geffen, A.J., Hansen, J.H., Helyar, S.J., Nielsen, E.E., Ogden, R., Patarnello, T., Stagioni, M., , Tinti, F. and Bargelloni, L., 2014. Outlier SNP markers reveal fine-scale genetic structuring across European hake populations (*Merluccius merluccius*). *Mol Ecol.* 23: 118-135. <https://doi.org/10.1111/mec.12568>
- Miller, K.A., Thompson, K.F., Johnston, P., Santillo, D., 2018. An Overview of Seabed Mining Including the Current State of Development, Environmental Impacts, and Knowledge Gaps. *Front. Mar. Sci.* 4, 418. <https://doi.org/10.3389/fmars.2017.00418>
- Mitarai, S., Siegel, D.A., Watson, J.R., Dong, C., McWilliams, J.C., 2009. Quantifying connectivity in the coastal ocean with application to the Southern California Bight. *J. Geophys. Res.* 114, C10026. <https://doi.org/10.1029/2008JC005166>

- Mitarai, S., Watanabe, H., Nakajima, Y., Shchepetkin, A.F., McWilliams, J.C., 2016. Quantifying dispersal from hydrothermal vent fields in the western Pacific Ocean. *Proc. Natl. Acad. Sci. U.S.A.* 113, 2976–2981. <https://doi.org/10.1073/pnas.1518395113>
- Monzier, M., Robin, C., Eissen, J-P, 1994. Kuwae (\approx 1425 A.D.): the forgotten caldera. *J. volcanol. Geotherm. Res.* 59, 207–218. [https://doi.org/10.1016/0377-0273\(94\)90091-4](https://doi.org/10.1016/0377-0273(94)90091-4)
- Mouchi, V., Pecheyran, C., Claverie, F., Cathalot, C., Matabos, M., Germain, Y., Rouxel, O., Jollivet, D., Broquet, T., Comtet, T., 2023. A step towards measuring connectivity in the deep-sea: elemental fingerprints of mollusk larval shells discriminate hydrothermal vent sites. *Biogeosciences*, 21, 145–160. *BioRxiv*. <https://doi.org/10.1101/2023.01.03.522618>
- Mullineaux, L.S., Adams, D.K., Mills, S.W., Beaulieu, S.E., 2010. Larvae from afar colonize deep-sea hydrothermal vents after a catastrophic eruption. *Proc. Natl. Acad. Sci. U.S.A.* 107, 7829–7834. <https://doi.org/10.1073/pnas.0913187107>
- Mullineaux, L.S., Metaxas, A., Beaulieu, S.E., Bright, M., Gollner, S., Grupe, B.M., Herrera, S., Kellner, J.B., Levin, L.A., Mitarai, S., Neubert, M.G., Thurnherr, A.M., Tunnicliffe, V., Watanabe, H.K., Won, Y.-J., 2018. Exploring the Ecology of Deep-Sea Hydrothermal Vents in a Metacommunity Framework. *Front. Mar. Sci.* 5, 49. <https://doi.org/10.3389/fmars.2018.00049>
- Murdock, S.A., Tunnicliffe, V., Boschen-Rose, R.E., Juniper, S.K., 2021. Emergent “core communities” of microbes, meiofauna and macrofauna at hydrothermal vents. *ISME COMMUN.* 1, 27. <https://doi.org/10.1038/s43705-021-00031-1>
- Nakasugi, F., Shimanaga, M., Nomaki, H., Watanabe, H.K., Kitahashi, T., Motomura, Y., Iseda, K., 2021. Simple harpacticoid composition observed at deep hydrothermal vent sites on sea knoll calderas in the North-west Pacific. *J. Mar. Biol. Ass.* 101, 947–956. <https://doi.org/10.1017/S0025315421000874>
- Nomaki, H., Kawatani, K., Motomura, Y., Tame, A., Uyeno, D., Ogawa, N.O., Ohkouchi, N., Shimanaga, M., 2023. Bacterivory of the hydrothermal-vent-specific copepod *Stygiopontius senokuchiae* (Dirivultidae, Siphonostomatoida) from copepodite through adult stages. *J. Mar. Biol. Ass.* 103, e21. <https://doi.org/10.1017/S0025315423000139>
- Nomaki, H., Uejima, Y., Ogawa, N., Yamane, M., Watanabe, H., Senokuchi, R., Bernhard, J., Kitahashi, T., Miyairi, Y., Yokoyama, Y., Ohkouchi, N., Shimanaga, M., 2019. Nutritional sources of meio- and macrofauna at hydrothermal vents and adjacent areas: natural-abundance radiocarbon and stable isotope analyses. *Mar. Ecol. Prog. Ser.* 622, 49–65. <https://doi.org/10.3354/meps13053>

- O'Connor, M.I., Bruno, J.F., Gaines, S.D., Halpern, B.S., Lester, S.E., Kinlan, B.P., Weiss, J.M., 2007. Temperature control of larval dispersal and the implications for marine ecology, evolution, and conservation. *Proc. Natl. Acad. Sci. U.S.A.* 104, 1266–1271. <https://doi.org/10.1073/pnas.0603422104>
- Olive, J.-A., Dublanchet, P., 2020. Controls on the magmatic fraction of extension at mid-ocean ridges. *Earth and Planetary Science Letters* 549, 116541. <https://doi.org/10.1016/j.epsl.2020.116541>
- Paris, J.R., Stevens, J.R., Catchen, J.M., 2017. Lost in parameter space: a road map for STACKS. *Methods Ecol Evol* 8, 1360–1373. <https://doi.org/10.1111/2041-210X.12775>
- Perez, M., Sun, J., Xu, Q., Qian, P.-Y., 2021. Structure and Connectivity of Hydrothermal Vent Communities Along the Mid-Ocean Ridges in the West Indian Ocean: A Review. *Front. Mar. Sci.* 8, 744874. <https://doi.org/10.3389/fmars.2021.744874>
- Petersen, S., Krätschell, A., Augustin, N., Jamieson, J., Hein, J.R., Hannington, M.D., 2016. News from the seabed – Geological characteristics and resource potential of deep-sea mineral resources. *Marine Policy* 70, 175–187. <https://doi.org/10.1016/j.marpol.2016.03.012>
- Pineda, J., Porri, F., Starczak, V., Blythe, J., 2010. Causes of decoupling between larval supply and settlement and consequences for understanding recruitment and population connectivity. *Journal of Experimental Marine Biology and Ecology* 392, 9–21. <https://doi.org/10.1016/j.jembe.2010.04.008>
- Poitrimol C, Thiébaud É, Daguin-Thiébaud C, Le Port A-S, Ballenghien M, Tran Lu Y A, Jollivet D, Hourdez S, Matabos M. Contrasted phylogeographic patterns of hydrothermal vent gastropods along South West Pacific: Woodlark Basin, a possible contact zone and/or stepping-stone. *PLoS ONE*. 2022 Oct 5; 17(10): e0275638. <https://doi.org/10.1371/journal.pone.0275638>
- Plouviez, S., LaBella, A.L., Weisrock, D.W., Von Meijenfeldt, F.A.B., Ball, B., Neigel, J.E., Van Dover, C.L., 2019. Amplicon sequencing of 42 nuclear loci supports directional gene flow between South Pacific populations of a hydrothermal vent limpet. *Ecol Evol* 9, 6568–6580. <https://doi.org/10.1002/ece3.5235>
- Plouviez, S., Schultz, T.F., McGinnis, G., Minshall, H., Rudder, M., Van Dover, C.L., 2013. Genetic diversity of hydrothermal-vent barnacles in Manus Basin. *Deep Sea Research Part I: Oceanographic Research Papers* 82, 73–79. <https://doi.org/10.1016/j.dsr.2013.08.004>
- Portanier, E., Nicolle, A., Rath, W., Monnet, L., Le Goff, G., Le Port, A.-S., Daguin-Thiébaud, C., Morrison, C.L., Cunha, M.R., Betters, M., Young, C.M., Van Dover, C.L., Biastoch, A., Thiébaud, E., Jollivet, D., 2023. Coupling large-spatial scale larval dispersal modelling with barcoding to refine the amphi-Atlantic connectivity hypothesis

- in deep-sea seep mussels. *Front. Mar. Sci.* 10, 1122124.
<https://doi.org/10.3389/fmars.2023.1122124>
- Posavi, M., Gelembiuk, G.W., Larget, B., Lee, C.E., 2014. Testing for beneficial reversal of dominance during salinity shifts in the invasive copepod *Eurytemora affinis*, and implications for the maintenance of genetic variation. *Evolution* 68, 3166–3183. <https://doi.org/10.1111/evo.12502>
- Riginos, C., Crandall, E.D., Liggins, L., Bongaerts, P., Trembl, E.A., 2016. Navigating the currents of seascape genomics: how spatial analyses can augment population genomic studies. *Curr Zool* 62, 581–601. <https://doi.org/10.1093/cz/zow067>
- Rochette, N.C., Catchen, J.M., 2017. Deriving genotypes from RAD-seq short-read data using Stacks. *Nat Protoc* 12, 2640–2659.
<https://doi.org/10.1038/nprot.2017.123>
- Rochette, N.C., Rivera-Colón, A.G., Catchen, J.M., 2019. Stacks 2: Analytical methods for paired-end sequencing improve RADseq-based population genomics. *Mol Ecol* 28, 4737–4754. <https://doi.org/10.1111/mec.15253>
- Rougeux, C., Bernatchez, L., Gagnaire, P.-A., 2017. Modeling the Multiple Facets of Speciation-with-Gene flow toward Inferring the Divergence History of Lake Whitefish Species Pairs (*Coregonus clupeaformis*). *Genome Biology and Evolution* 9, 2057–2074. <https://doi.org/10.1093/gbe/evx150>
- Ruellan, E., Delteil, J., Wright, I., Matsumoto, T., 2003. From rifting to active spreading in the Lau Basin - Havre Trough backarc system (SW Pacific): Locking/unlocking induced by seamount chain subduction: LAU BASIN-HAVRE TROUGH SYSTEM. *Geochem. Geophys. Geosyst.* 4, n/a-n/a.
<https://doi.org/10.1029/2001GC000261>
- Siberchicot, A., Julien-Laferrrière, A., Dufour, A., Thioulouse, J., Dray, S., 2017. adegraphics: An S4 Lattice-Based Package for the Representation of Multivariate Data. *The R Journal*. 9 (2):198-212. <https://doi.org/10.32614/RJ-2017-042>
- Siegel, D.A., Kinlan, B.P., Gaylord, B. and Gaines, S.D., 2003. Lagrangian descriptions of marine larval dispersion. *Marine Ecology Progress Series*, 260, pp.83-96.
<https://doi.org/10.3354/meps260083>
- Simons, E., Speer, K., Thurnherr, A.M., 2019. Deep circulation in the Lau Basin and Havre Trough of the western South Pacific Ocean from floats and hydrography. *J mar res* 77, 353–374. <https://doi.org/10.1357/002224019833406150>
- Smagorinsky, J., 1963. GENERAL CIRCULATION EXPERIMENTS WITH THE PRIMITIVE EQUATIONS: I. THE BASIC EXPERIMENT*. *Mon. Wea. Rev.* 91, 99–164.
[https://doi.org/10.1175/1520-0493\(1963\)091<0099:GCEWTP>2.3.CO;2](https://doi.org/10.1175/1520-0493(1963)091<0099:GCEWTP>2.3.CO;2)

- Speer, K., Thurnherr, A., 2012b. The Lau Basin Float Experiment (LAUB-FLEX). *oceanog* 25, 284–285. <https://doi.org/10.5670/oceanog.2012.27>
- Stewart, M.S., Hannington, M.D., Emberley, J., Baxter, A.T., Krätschell, A., Petersen, S., Brandl, P.A., Anderson, M.O., Mercier-Langevin, P., Mensing, R., Breker, K., Fassbender, M.L., 2022. A new geological map of the Lau Basin (southwestern Pacific Ocean) reveals crustal growth processes in arc-backarc systems. *Geosphere*. <https://doi.org/10.1130/GES02340.1>
- Storey, J.D., 2003. The positive false discovery rate: a Bayesian interpretation and the q-value. *Ann. Statist.* 31. <https://doi.org/10.1214/aos/1074290335>
- Sunde, J., Yıldırım, Y., Tibblin, P., Forsman, A., 2020. Comparing the Performance of Microsatellites and RADseq in Population Genetic Studies: Analysis of Data for Pike (*Esox lucius*) and a Synthesis of Previous Studies. *Front. Genet.* 11, 218. <https://doi.org/10.3389/fgene.2020.00218>
- Sundqvist, L., Keenan, K., Zackrisson, M., Prodöhl, P., Kleinhans, D., 2016. Directional genetic differentiation and relative migration. *Ecol Evol* 6, 3461–3475. <https://doi.org/10.1002/ece3.2096>
- Teixeira, S., Cambon-Bonavita, M.-A., Serrão, E.A., Desbruyères, D., Arnaud-Haond, S., 2011. Recent population expansion and connectivity in the hydrothermal shrimp *Rimicaris exoculata* along the Mid-Atlantic Ridge: Genetic diversity of a hydrothermal vent shrimp. *Journal of Biogeography* 38, 564–574. <https://doi.org/10.1111/j.1365-2699.2010.02408.x>
- Teixeira, S., Serrão, E.A., Arnaud-Haond, S., 2012. Panmixia in a Fragmented and Unstable Environment: The Hydrothermal Shrimp *Rimicaris exoculata* Disperses Extensively along the Mid-Atlantic Ridge. *PLoS ONE* 7, e38521. <https://doi.org/10.1371/journal.pone.0038521>
- Tepper, B., Bradley, B.P., 1989. Temporal Changes in a Natural Population of Copepods. *The Biological Bulletin* 176, 32–40. <https://doi.org/10.2307/1541886>
- Thaler, A.D., Plouviez, S., Saleu, W., Alei, F., Jacobson, A., Boyle, E.A., Schultz, T.F., Carlsson, J., Van Dover, C.L., 2014. Comparative Population Structure of Two Deep-Sea Hydrothermal-Vent-Associated Decapods (*Chorocaris* sp. 2 and *Munidopsis lauensis*) from Southwestern Pacific Back-Arc Basins. *PLoS ONE* 9, e101345. <https://doi.org/10.1371/journal.pone.0101345>
- Thomas, G.W.C., Dohmen, E., Hughes, D.S.T., Murali, S.C., Poelchau, M., Glastad, K., Anstead, C.A., Ayoub, N.A., Batterham, P., Bellair, M., Binford, G.J., Chao, H., Chen, Y.H., Childers, C., Dinh, H., Doddapaneni, H.V., Duan, J.J., Dugan, S., Esposito, L.A., Friedrich, M., Garb, J., Gasser, R.B., Goodisman, M.A.D., Gundersen-Rindal, D.E., Han, Y., Handler, A.M., Hatakeyama, M., Hering, L., Hunter, W.B., Ioannidis, P.,

- Jayaseelan, J.C., Kalra, D., Khila, A., Korhonen, P.K., Lee, C.E., Lee, S.L., Li, Y., Lindsey, A.R.I., Mayer, G., McGregor, A.P., McKenna, D.D., Misof, B., Munidasa, M., Munoz-Torres, M., Muzny, D.M., Niehuis, O., Osuji-Lacy, N., Palli, S.R., Panfilio, K.A., Pechmann, M., Perry, T., Peters, R.S., Poynton, H.C., Prpic, N.-M., Qu, J., Rotenberg, D., Schal, C., Schoville, S.D., Scully, E.D., Skinner, E., Sloan, D.B., Stouthamer, R., Strand, M.R., Szucsich, N.U., Wijeratne, A., Young, N.D., Zattara, E.E., Benoit, J.B., Zdobnov, E.M., Pfrender, M.E., Hackett, K.J., Werren, J.H., Worley, K.C., Gibbs, R.A., Chipman, A.D., Waterhouse, R.M., Bornberg-Bauer, E., Hahn, M.W., Richards, S., 2020. Gene content evolution in the arthropods. *Genome Biol* 21, 15. <https://doi.org/10.1186/s13059-019-1925-7>
- Tran Lu Y, A., Ruault, S., Daguin-Thiébaud, C., Castel, J., Bierne, N., Broquet, T., Wincker, P., Perdereau, A., Arnaud-Haond, S., Gagnaire, P., Jollivet, D., Hourdez, S., Bonhomme, F., 2022. Subtle limits to connectivity revealed by outlier loci within two divergent metapopulations of the deep-sea hydrothermal gastropod *Ifremeria nautili*. *Molecular Ecology* 31, 2796–2813. <https://doi.org/10.1111/mec.16430>
- Tripp, E.A., Tsai, Y.E., Zhuang, Y., Dexter, K.G., 2017. RAD seq dataset with 90% missing data fully resolves recent radiation of *Petalidium* (Acanthaceae) in the ultra-arid deserts of Namibia. *Ecol Evol* 7, 7920–7936. <https://doi.org/10.1002/ece3.3274>
- Tsurumi, M., De Graaf, R.C., Tunncliffe, V., 2003. Distributional and Biological Aspects of Copepods at Hydrothermal Vents on the Juan de Fuca Ridge, north-east Pacific Ocean. *J. Mar. Biol. Ass.* 83, 469–477. <https://doi.org/10.1017/S0025315403007367h>
- Van Dover, C.L., 2014. Impacts of anthropogenic disturbances at deep-sea hydrothermal vent ecosystems: A review. *Marine Environmental Research* 102, 59–72. <https://doi.org/10.1016/j.marenvres.2014.03.008>
- Van Dover, C.L., Arnaud-Haond, S., Gianni, M., Helmreich, S., Huber, J.A., Jaeckel, A.L., Metaxas, A., Pendleton, L.H., Petersen, S., Ramirez-Llodra, E., Steinberg, P.E., Tunncliffe, V., Yamamoto, H., 2018. Scientific rationale and international obligations for protection of active hydrothermal vent ecosystems from deep-sea mining. *Marine Policy* 90, 20–28. <https://doi.org/10.1016/j.marpol.2018.01.020>
- Virtanen, E.A., Moilanen, A., Viitasalo, M., 2020. Marine connectivity in spatial conservation planning: analogues from the terrestrial realm. *Landscape Ecol* 35, 1021–1034. <https://doi.org/10.1007/s10980-020-00997-8>
- Vrijenhoek, R. C., 2010. Genetic diversity and connectivity of deep-sea hydrothermal vent metapopulations. *Mol. Ecol.* 19: 4391–4411. <https://doi.org/10.1111/j.1365-294X.2010.04789.x>

- Wang, S., Meyer, E., McKay, J.K., Matz, M.V., 2012. 2b-RAD: a simple and flexible method for genome-wide genotyping. *Nat Methods* 9, 808–810.
<https://doi.org/10.1038/nmeth.2023>
- Watanabe, H.K., Senokuchi, R., Nomaki, H., Kitahashi, T., Uyeno, D., Shimanaga, M., 2021. Distribution and Genetic Divergence of Deep-Sea Hydrothermal Vent Copepods (Dirivultidae: Siphonostomatoida: Copepoda) in the Northwestern Pacific. *Zoological Science* 38. <https://doi.org/10.2108/zs200153>
- Won, Y., Hallam, S.J., O'Mullan, G.D., Vrijenhoek, R.C., 2003. Cytonuclear disequilibrium in a hybrid zone involving deep-sea hydrothermal vent mussels of the genus *Bathymodiolus*. *Molecular Ecology* 12, 3185–3190.
<https://doi.org/10.1046/j.1365-294X.2003.01974.x>
- Xu, T., Wang, Y., Sun, J., Chen, C., Watanabe, H.K., Chen, J., Qian, P.-Y., Qiu, J.-W., 2021. Hidden Historical Habitat-Linked Population Divergence and Contemporary Gene Flow of a Deep-Sea Patellogastropod Limpet. *Molecular Biology and Evolution* 38, 5640–5654. <https://doi.org/10.1093/molbev/msab278>
- Xuereb, A., Benestan, L., Normandeau, É., Daigle, R.M., Curtis, J.M.R., Bernatchez, L., Fortin, M.-J., 2018. Asymmetric oceanographic processes mediate connectivity and population genetic structure, as revealed by RADseq, in a highly dispersive marine invertebrate (*Parastichopus californicus*). *Mol Ecol* 27, 2347–2364.
<https://doi.org/10.1111/mec.14589>
- Yahagi, T., Fukumori, H., Warén, A., & Kano, Y., 2019. Population connectivity of hydrothermal-vent limpets along the northern Mid-Atlantic Ridge (Gastropoda: Neritimorpha: Phenacolepadidae). *Journal of the Marine Biological Association of the United Kingdom*, 99(1), 179–185.
<https://doi.org/10.1017/S0025315417001898>
- Yahagi, T., Kayama Watanabe, H., Kojima, S., Kano, Y., 2017. Do larvae from deep-sea hydrothermal vents disperse in surface waters? *Ecology* 98, 1524–1534.
<https://doi.org/10.1002/ecy.1800>
- Yahagi, T., Thaler, A.D., Van Dover, C.L., Kano, Y., 2020. Population connectivity of the hydrothermal-vent limpet *Shinkailepas tollmanni* in the Southwest Pacific (Gastropoda: Neritimorpha: Phenacolepadidae). *PLoS ONE* 15, e0239784.
<https://doi.org/10.1371/journal.pone.0239784>
- Yearsley, J.M., Salmanidou, D.M., Carlsson, J., Burns, D., Van Dover, C.L., 2020. Biophysical models of persistent connectivity and barriers on the northern Mid-Atlantic Ridge. *Deep Sea Research Part II: Topical Studies in Oceanography* 180, 104819. <https://doi.org/10.1016/j.dsr2.2020.104819>

1657 Table 1: Location of sampling sites (latitude and longitude) with corresponding depth (m) at time of
1658 sampling. Spreading rate values were taken from Stewart et al. (2022).
1659

Basin	Site	Latitude	Longitude	Depth (m)	Spreading Rate	Substrate	Sample size	Year sampled	References
ELSC	Tu'i Malila	-21.99	-176.57	1888	48	Basalt	24	2019	Hourdez and Jollivet (2019) Stewart et al. (2022)
ELSC	ABE	-20.76	-176.19	2155	69	Andesitic	24	2016	Beinart et al. (2018) Stewart et al. (2022)
ELSC	ABE	-20.77	-176.20	2153	69	Andesitic	11	2019	Hourdez and Jollivet (2019) Stewart et al. (2022)
ELSC	Tahi Moana	-20.05	-176.13	2273	69	Andesitic	15	2016	Beinart et al. (2018) Stewart et al. (2022)
ELSC	Mangatolo	-15.41	185.35	2039	37	Andesitic	64	2019	Hourdez and Jollivet (2019) Stewart et al. (2022)

1660
1661
1662
1663

1664 Table 2: Analysis of Molecular Variance results of pairwise differences between populations, indicating the
1665 pairs, the Fst value for each pair and the *p*-value associated with each Fst calculation. Significance codes:
1666 (**p < 0.001, *p < 0.01 *p < 0.05). Observed heterozygosity for each population was calculated (Het_{obs}).
1667

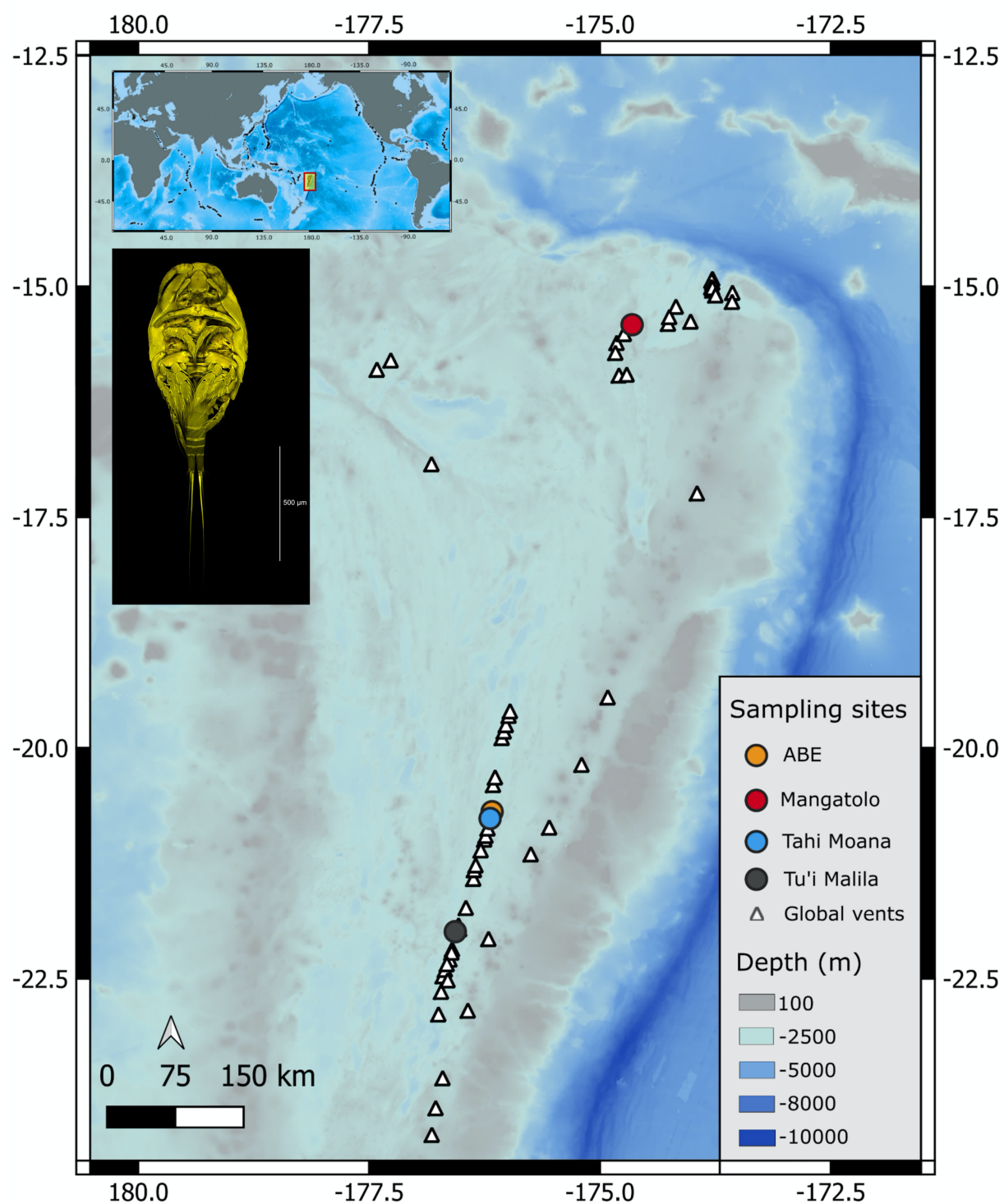
Population	Het _{obs}	Tahi Moana	Mangatolo	Tui Malila	ABE (2016)	ABE (2019)
Tahi Moana	0.12	0				
Mangatolo	0.24	0.24*	0			
Tui Malila	0.18	0.24*	0.12*	0		
ABE (2016)	0.12	0.00	0.26*	0.25*	0	
ABE (2019)	0.08	0.11*	0.05*	0.08*	0.07*	0

1668
1669
1670
1671
1672
1673
1674
1675
1676
1677

Table 3: Parameters estimated from $\partial a \partial i$ for the best model (SC2N2mG) with their standard deviations (SD) estimated using the Fisher Information Matrix (FIM), and with parameters describing effective population size (2N), migration rate (2m), and population growth (G) between populations within the Lau basin.

North-mid			North-south		
Parameter	Value	SD	Parameter	Value	SD
Nu1 (mid)	2.41	0.63	Nu1 (north)	1.40	0.76
Nu2 (north)	0.80	0.61	Nu2 (south)	1.24	1.16
b1	0.31	0.07	b1	0.74	0.21
b2	0.63	0.60	b2	1.03	0.19
hrf	0.14	0.07	hrf	0.11	0.06
T _s	4.91	1.47	T _s	7.92	5.80
T _{sc}	0.17	0.01	T _{sc}	0.26	0.07
m1<-2	0.68	0.10	m1<-2	5.24	1.16
m2<-1	5.97	0.40	m2<-1	6.24	2.35
me1<-2	0.98	0.09	me1<-2	4.64	1.39
me2<-1	0.51	0.13	me2<-1	1.03	0.64
P	0.74	0.04	P	0.03	0.23
Q	0.17	0.12	Q	0.49	0.28
Theta	91.82	23.55	Theta	155.82	93.60
Time to population split (years)	119,422	35,764	Time to the population split (years)	325,661	239,304
Time to secondary contact (years)	4,050	274	Time to the secondary contact (years)	10,762	3,231

1684



1685

1686 Figure 1: Map of sampling sites from 2016, and 2019 within the Lau Basin (Mangatolo, Tahi Moana, ABE,
 1687 and Tu'i Malila). A dorsal confocal microscopic image of an *S. lauensis* female from the ABE hydrothermal
 1688 vent field in the Lau Basin. Image taken at the German Center for Marine Biodiversity Research by Dr. Jimmy
 1689 Bernot.
 1690

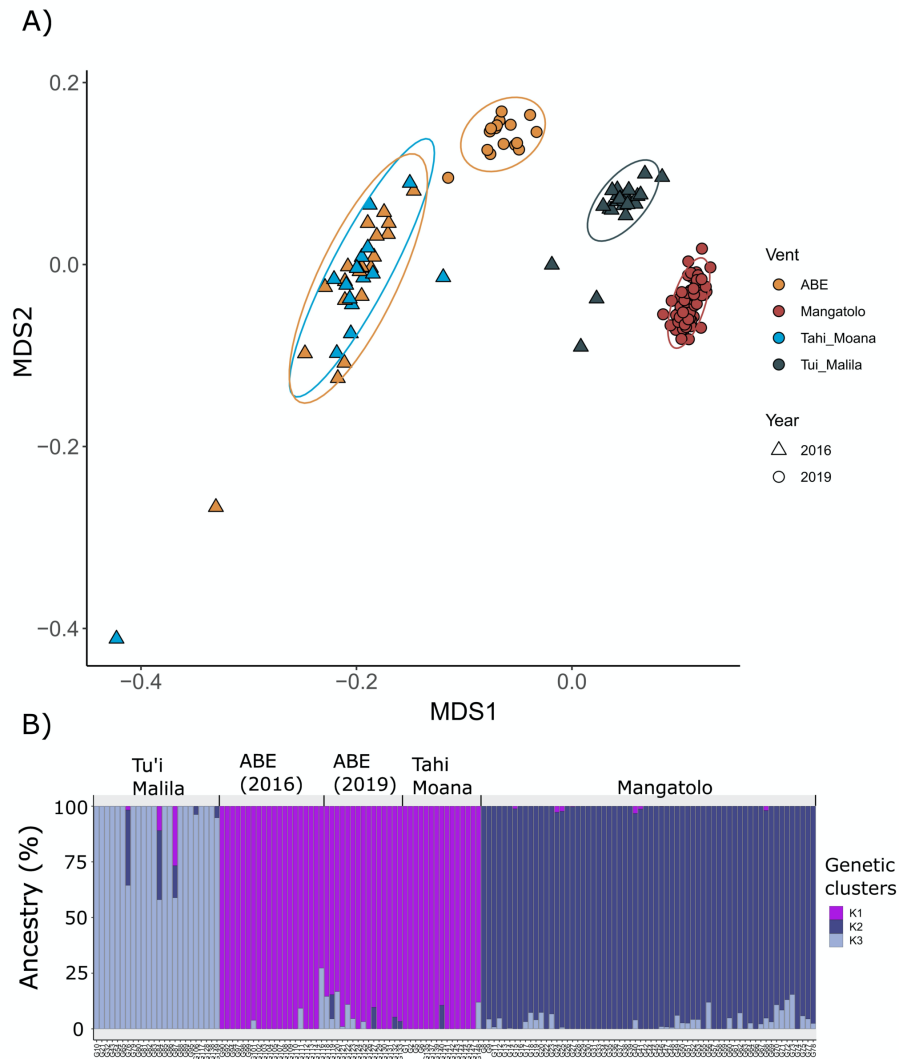


Figure 2: Structure of populations of *S. lauensis* in the Lau Basin. A) non-Metric Multidimensional Scaling (nMDS), where data is coloured by vent site and shapes denote the sampling year (open circles = 2019, hatched square = 2016). Ellipsoids represent 95 % confidence intervals. B) ADMIXTURE plots for each individual coloured by ancestry and grouped by sampling site/population for the optimal $K=3$.

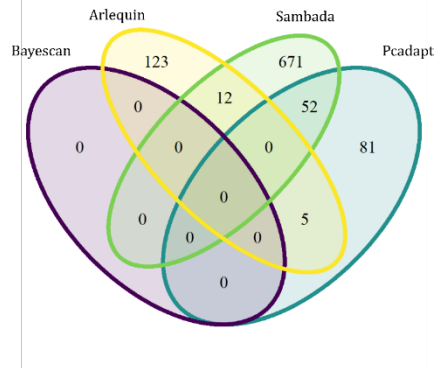
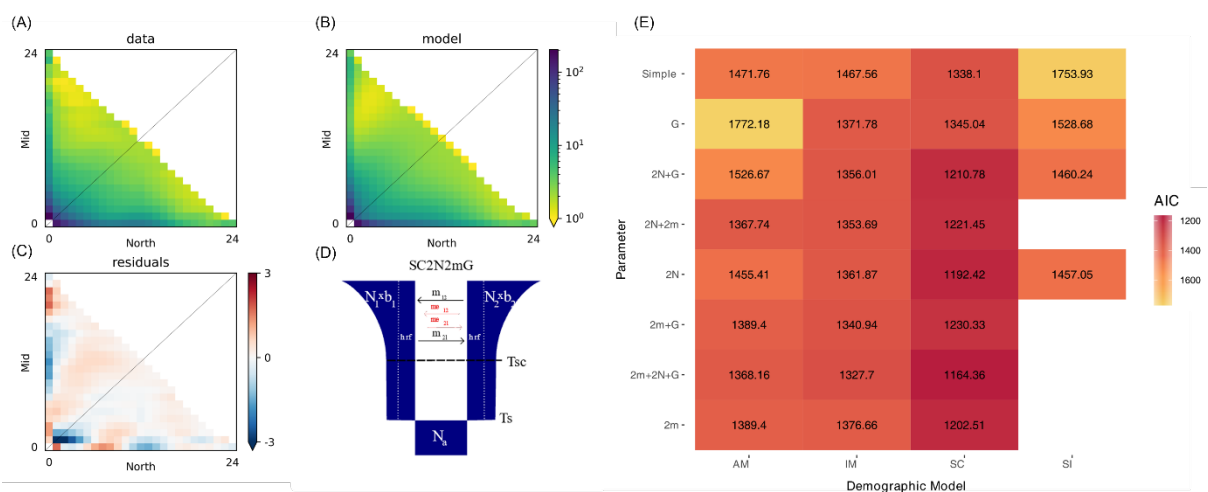
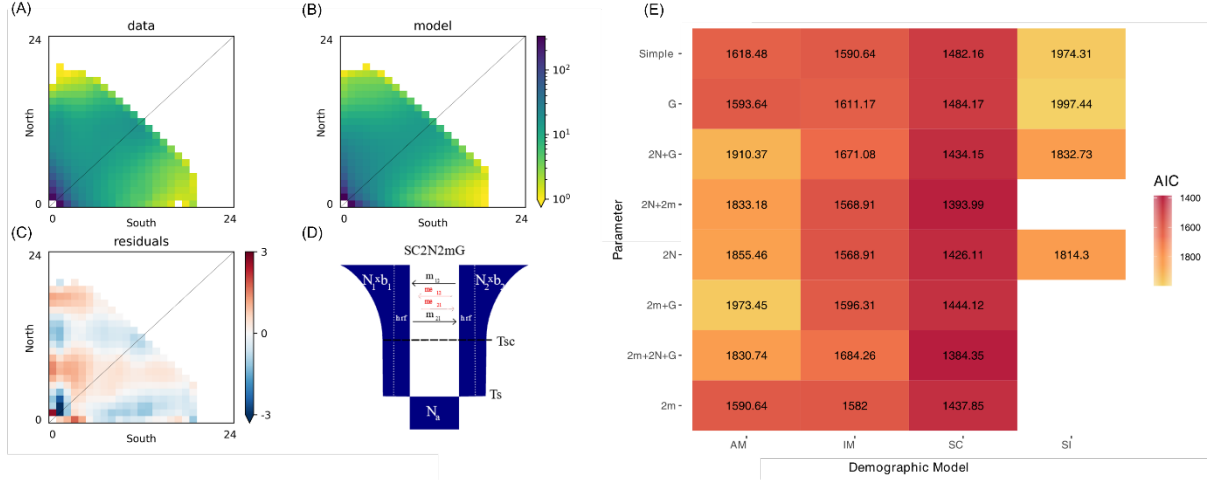


Figure 3: Venn diagram of outlier SNPs (unique and shared) found by the different outlier detection software Bayescan, Arlequin, Sambada, and PCAdapt.



1711
1712
1713
1714
1715
1716
1717
1718
1719

Figure 4: A) Joint allele frequency spectrum (JAFS) between North (Mangatolo) and Mid (pooled Tahi Moana and ABE) vent sites within the Lau Basin. B) Simulated JAFS under the SC2N2mG model. The log scale indicates the density of SNPs in each frequency class (shared between the mid and north). C) Residuals of the fit of the simulated model on the data. D) Schematic of the fitted model (N , population size; b , population growth factor; h , the Hill-Robertson factor, which simulates linked selection; m , unrestricted migration rate; m_e , restricted migration rate, which simulates barrier loci). E) Heat-map of the best Akaike information criterion (AIC) value for each parameter combination (population expansion or contraction [G], effect of linked selection [$2N$] and heterogeneous migration [$2m$]) and demographic model (strict isolation [SI], isolation with migration [IM], ancient migration [AM], and secondary contact [SC]).



1721
1722
1723
1724
1725
1726
1727
1728
1729
1730
1731
1732

Figure 5: A) Joint allele frequency spectrum (JAFS) between North (Mangatolo) and South (Tu'i Malila) vent sites within the Lau Basin. B) Simulated JAFS under the SC2N model. The log scale indicates the density of SNPs in each frequency class. C) Residuals of the fit of the simulated model on the data. D) Schematic of the fitted model (N , population size; b , population growth factor; h , the Hill-Robertson factor, which simulates linked selection; m , unrestricted migration rate; m_e , restricted migration rate, which simulates barrier loci). E) Heat-map of the best Akaike information criterion (AIC) value for each parameter combination (population expansion or contraction [G], effect of linked selection [$2N$] and heterogeneous migration [$2m$]) and demographic model (strict isolation [SI], isolation with migration [IM], ancient migration [AM], and secondary contact [SC]).

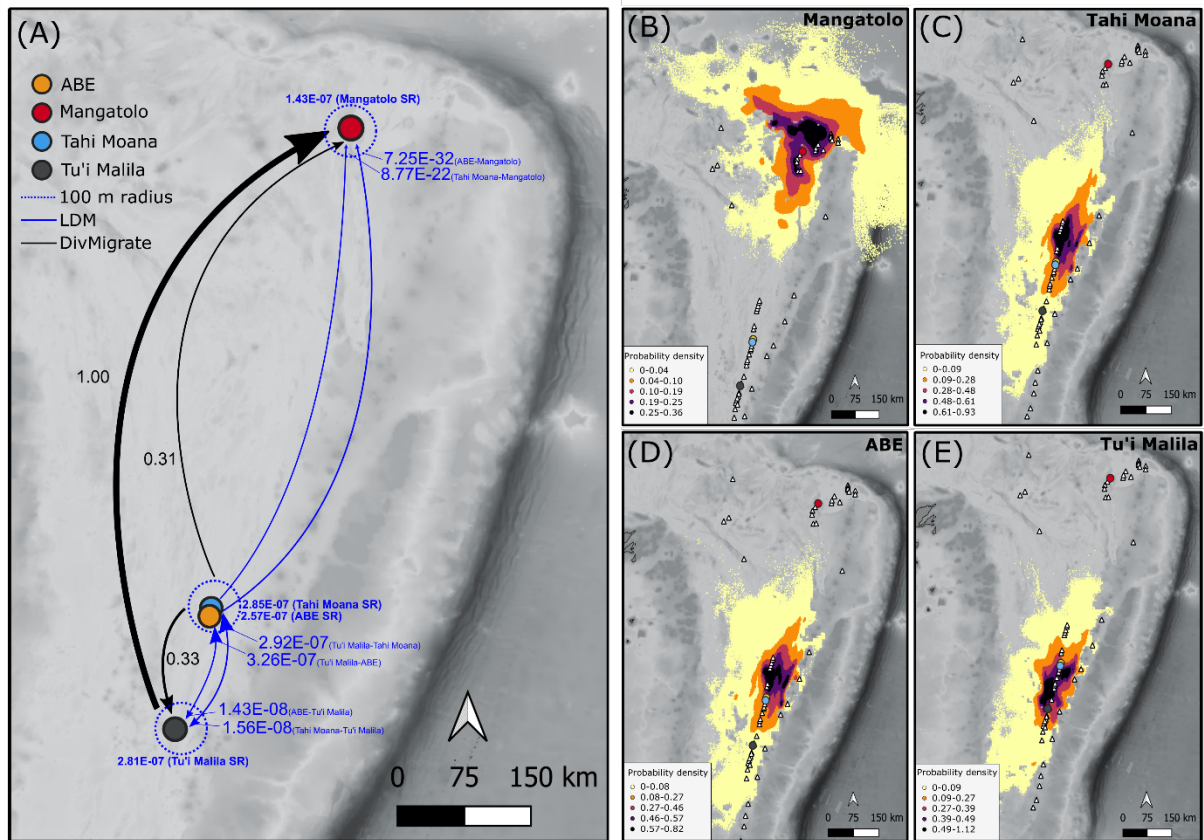


Figure 6: A) Significant relative migration (effective number of migrants, nM) calculated using the Nm statistic and 1000 bootstraps in *DivMigrate* (empirical data = black arrows), and larval dispersal model (LDM) simulations (blue arrows). Blue dashed line denotes a 100 m radius (not to scale around each vent). The thickness of the arrows and size of the arrow heads in each instance denotes the strength of directionality. SR = self-recruitment. Gaussian point distribution probabilities (probability density) for B) Mangatolo, C) Tahi Moana, D) ABE, and E) Tu'i Malila. Blue dashed White triangles denote existing (and possibly stepping stone) vents within the basin from which data was not collected.